Implementation of a Silver Iodide Cloud-Seeding Parameterization in WRF. Part I: Model Description and Idealized 2D Sensitivity Tests

LULIN XUE

National Center for Atmospheric Research, Boulder, Colorado*

AKIHIRO HASHIMOTO AND MASATAKA MURAKAMI

Meteorological Research Institute, Tsukuba, Ibaraki, Japan

ROY RASMUSSEN, SARAH A. TESSENDORF, AND DANIEL BREED

National Center for Atmospheric Research, Boulder, Colorado

SHAUN PARKINSON, PAT HOLBROOK, AND DEREK BLESTRUD

Idaho Power Company, Boise, Idaho

(Manuscript received 5 June 2012, in final form 26 November 2012)

ABSTRACT

A silver iodide (AgI) cloud-seeding parameterization has been implemented into the Thompson microphysics scheme of the Weather Research and Forecasting model to investigate glaciogenic cloud-seeding effects. The sensitivity of the parameterization to meteorological conditions, cloud properties, and seeding rates was examined by simulating two-dimensional idealized moist flow over a bell-shaped mountain. The results verified that this parameterization can reasonably simulate the physical processes of cloud seeding with the limitations of the constant cloud droplet concentration assumed in the scheme and the two-dimensional model setup. The results showed the following: 1) Deposition was the dominant nucleation mode of AgI from simulated aircraft seeding, whereas immersion freezing was the most active mode for ground-based seeding. Deposition and condensation freezing were also important for ground-based seeding. Contact freezing was the weakest nucleation mode for both ground-based and airborne seeding. 2) Diffusion and riming on AgI-nucleated ice crystals depleted vapor and liquid water, resulting in more ice-phase precipitation on the ground for all of the seeding cases relative to the control cases. Most of the enhancement came from vapor depletion. The relative enhancement by seeding ranged from 0.3% to 429% under various conditions. 3) The maximum local AgI activation ratio was 60% under optimum conditions. Under most seeding conditions, however, this ratio was between 0.02% and 2% in orographic clouds. 4) The seeding effect was inversely related to the natural precipitation efficiency but was positively related to seeding rates. 5) Ground-based seeding enhanced precipitation on the lee side of the mountain, whereas airborne seeding from lower flight tracks enhanced precipitation on the windward side of the mountain.

1. Introduction

Freshwater is becoming one of the most stressed and in-demand natural resources given the rapidly increasing human population. The need for water provides motivation to find solutions other than drilling wells, digging canals, and building reservoirs. Cloud seeding is

*The National Center for Atmospheric Research is sponsored by the National Science Foundation.

Corresponding author address: Lulin Xue, National Center for Atmospheric Research, P.O. Box 3000, Boulder, CO 80307.
E-mail: xuel@ucar.edu

DOI: 10.1175/JAMC-D-12-0148.1

one method being pursued in many locations around the world. Since the first proof-of-concept experiment on glaciogenic seeding of nonprecipitating supercooled stratus clouds by dry ice (Schaefer 1946) and the discovery of the ice nucleation ability of silver iodide (Vonnegut 1947), many glaciogenic cloud-seeding operational programs and field campaigns have been carried out worldwide over the last several decades (Bruintjes 1999; Qiu and Cressey 2008).

Despite the varieties of seeding materials being used, seeding methods being applied, and cloud regimes being seeded in these programs, the effect of cloud seeding in enhancing precipitation on the ground is still largely inconclusive (National Research Council 2003). The difficulties in evaluating cloud-seeding effects are attributed to the following reasons: 1) the seeding signals are often very weak so that they are difficult to detect in natural precipitation with high variability; 2) the spatial and temporal scales of cloud-seeding effects may be different from those of seeding operations, especially in conjunction with significant dynamic effects; 3) the repeatability of real seeding activities under controlled environments is infeasible; 4) the cost of programs to evaluate the effects of cloud seeding is very high (e.g., randomized-seeding experiments).

Evaluating the seeding effect is typically done by weighing physical and/or statistical evidence (Bruintjes 1999). Physical measurements aimed at verifying the steps in the chain of events that lead to precipitation formation make up the physical evidence and include the detection of silver iodide (AgI) plumes released from the ground-based generators in the cloud region, the concentration of ice crystals and snowflakes in clouds overlapping with AgI plumes, and the detection of AgI inside the snow on the ground. Many previous experiments have successfully documented the dispersion of AgI plumes and the associated microphysical changes in orographic clouds (e.g., Super and Heimbach 1988; Super and Boe 1988; Deshler et al. 1990; Holroyd et al. 1995; Super 1999; Huggins 2007) and the detections of silver in snowpack over target areas (Warburton et al. 1995a,b). These studies generally analyzed individual cases rather than a group of events. Geerts et al. (2010) more recently applied a high-resolution, vertically pointing, millimeter-wave airborne Doppler radar to investigate wintertime glaciogenic seeding effects for seven cases in Wyoming. Their results showed that the increase in near-surface reflectivity is attributed to AgI seeding with statistical significance. Those results should be interpreted with caution given the large natural variability of meteorological conditions and the small population of the cases.

Statistical evaluations involve the measurement of precipitation on the ground as the response variable to seeding activities. In general, a fixed target–control design (Dennis 1980) and the randomized-seeding technique are used in modern confirmatory cloud-seeding experiments, especially wintertime orographic glaciogenic cloud-seeding programs. The Snowy Precipitation Enhancement Research Project (SPERP) undertaken in winters from 2005 to 2009 in southeastern Australia is one such experiment (Manton et al. 2011; Manton and Warren 2011). A positive, but not statistically significant, impact on precipitation by ground-based AgI seeding was found. The analyses on subsets of the longer seeding cases indicated higher significance levels being achieved. The Wyoming Weather Modification Pilot Program (WWMPP) is another recent outcome-focused randomized program (Breed et al. 2011). The WWMPP is an ongoing project from 2005 that applied a randomized crossover design (Gabriel 1999) to reduce the variance and the required sample size, assuming a positive correlation between precipitation at the two sites.

In addition to physical evaluations of the cloud-seeding efficacy, numerical models are useful tools to assist a seeding program in choosing the cases and identifying potential areas that will be affected by seeding. The SPERP used the ''GUIDE'' dispersion model (Rauber et al. 1988) to guide the operations of ground-based generators. A customized Real-Time Four Dimensional Data Assimilation (RTFDDA) version of the Weather Research and Forecasting (WRF) model (Liu et al. 2008) was deployed in the WWMPP to provide real-time high-resolution (every 3 h on a domain with 2-km grid spacing) weather and AgI trajectory forecasts. Forecasters using the model outputs found the information to be useful in calling seeding operations (B. Boe 2012, personal communication).

The first demonstration of a numerical model's capability to simulate the cloud-seeding effect in three dimensions (3D) was presented in Meyers et al. (1995). The four ice nucleation modes (deposition, condensation freezing, contact freezing, and immersion freezing) of AgI particles were parameterized according to the laboratory work by DeMott (1995) into the Regional Atmospheric Modeling System. They performed a high-resolution simulation (1-km horizontal grid spacing) of an orographic seeding case from December of 1986 from the Sierra Cooperative Pilot Project (Reynolds and Dennis 1986). Their results showed that the model reasonably simulated the physical chain of events associated with seeding and found precipitation enhancements that were similar to values inferred from the observations. Many numerical investigations on seeding effects have been performed since then (e.g., Reisin et al. 1996; Li and Pitter 1997; Yin et al. 2000; Guo et al. 2006; Curic et al. 2007; Chen and Xiao 2010) using different AgI

nucleation parameterizations and/or different model setups. Seeding effects on precipitation enhancement were found to be positive in most studies, and seeding was shown to change the precipitation distribution most of the time. Most of these studies dealt with convective cloud-seeding scenarios, however. Few numerical studies examined in a systematic way the sensitivities of seeding effects on wintertime orographic clouds to meteorological conditions and cloud microphysical properties (Li and Pitter 1997) even though the orographic cloud was identified as one of the most susceptible cloud types to anthropogenic pollution and artificial cloud seeding (Givati and Rosenfeld 2005).

In the past several decades, computer technology has continued to advance and numerical models have come to an era in which it is possible to simulate real atmospheric events in great detail—a situation that was not previously available. By implementing an AgI cloud-seeding parameterization that is based on Meyers et al. (1995) and DeMott (1995) into the WRF model, this two-part series investigates how simulated seeding effects are affected by the meteorological environments and varying cloud properties under both idealized and realistic conditions. The potential of evaluating glaciogenic cloud-seeding effects on wintertime orographic clouds by combining field observations and numerical simulations is demonstrated as well. This paper series tries to bridge the gap of knowledge in cloud seeding by improving the numerical component as was suggested by the National Research Council (2003).

Part I (this paper) of this two-part article focuses on demonstrating the ability of the parameterization to reasonably simulate the chain of events that is associated with precipitation formation and cloud seeding while investigating in two dimensions (2D) the sensitivity of seeding effects to environments and cloud properties. We do not intend to reproduce real seeding events in Part I but rather to use these idealized simulations to investigate the physics associated with cloud seeding. The parameterizations of different AgI nucleation modes are described in section 2; the experimental design and WRF model setups of the 2D idealized sensitivity tests are presented in section 3. Results are provided in section 4 and are followed by discussion in section 5. The conclusions are summarized in section 6.

2. Description of the AgI cloud-seeding parameterization

A silver iodide cloud-seeding parameterization has been implemented in the Thompson microphysics scheme (Hashimoto et al. 2008). The Thompson scheme proved to be very realistic in simulating and forecasting wintertime precipitation events (e.g., Thompson et al. 2004, 2008; Rasmussen et al. 2011; Liu et al. 2011). The AgI fraction of nucleating ice crystals by four ice nucleation modes: deposition F_{dep}, condensation freezing F_{cdf}, contact freezing F_{ctf}, and immersion freezing F_{imf}, are parameterized following DeMott (1995) and Meyers et al. (1995).

For deposition nucleation,

$$F_{\text{dep}} = a(S_i - 1) + b\left(\frac{273.16 - T}{T_0}\right) + c(S_i - 1)^2 + d\left(\frac{273.16 - T}{T_0}\right)^2 + e(S_i - 1)^3, \quad (1)$$

where $T_0 = 10.0\,\text{K}$, $a = -3.25 \times 10^{-3}$, $b = 5.39 \times 10^{-5}$, $c = 4.35 \times 10^{-2}$, $d = 1.55 \times 10^{-4}$, and $e = -0.07$. Here, S_i is ice saturation ratio and T is temperature in kelvins. This equation is valid when $S_i > 1.04$ and $T < 268.2\,\text{K}$.

For condensation-freezing nucleation,

$$F_{\text{cdf}} = a\left(\frac{268.66 - T}{T_0}\right)^3 (S_w - 1)^2, \quad (2)$$

where $T_0 = 10.0\,\text{K}$, $a = 900.0$, and S_w is water saturation ratio. This equation is valid when $T < 268.66\,\text{K}$ and $S_w > 1.0$.

For contact-freezing nucleation,

$$F_{\text{ctf}} = F_{\text{scav}}[a + b(S_i - 1) + c(S_i - 1)^2 + d(S_i - 1)^3 + e(S_i - 1)^4 + f(S_i - 1)^5 + g(S_i - 1)^6], \quad (3)$$

where $a = 0.0878$, $b = -3.7947$, $c = 52.3167$, $d = -255.4484$, $e = 568.3257$, $f = -460.4234$, and $g = -63.1248$. Here, F_{scav} is the fraction of the total AgI particles that is scavenged by liquid drops. The term F_{scav} includes the collection of AgI particles by cloud droplets through Brownian diffusion, turbulent diffusion, and phoretic effects (thermophoresis and diffusiophoresis). Impact scavenging of AgI particles by rain drops is not considered in this case because the AgI particles are too small to be effectively collected by these large drops. The detailed formulations of F_{scav} follow Caro et al. (2004). In addition to scavenging of AgI by droplets, a similar scavenging process of AgI by ice crystals is also considered in the parameterization. Equation (3) is valid when $S_i > 1.058$ and $T < 269.2\,\text{K}$.

For immersion-freezing nucleation,

$$F_{\text{imf}} = a(F_{\text{imm}})\left(\frac{268.2 - T}{T_0}\right)^b, \quad (4)$$

where $T_0 = 10.0\,\text{K}$, $a = 0.0274$, and $b = 3.3$. This form is valid when $T < 268.2\,\text{K}$. The term F_{imm} is the fraction

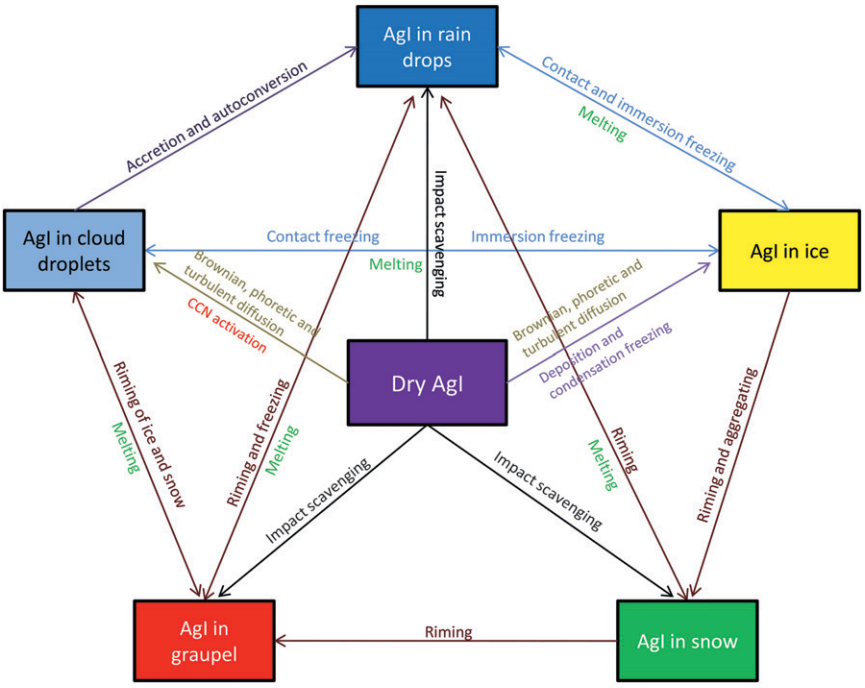

FIG. 1. Schematic of the AgI–cloud interactions that are simulated in the seeding parameterization.

of nonactivated AgI immersed in drops, which is determined by tracking the scavenged AgI number and the tendencies of microphysical processes that are associated with AgI-containing hydrometeors.

In addition to scavenging of AgI particles by nucleation and Brownian, phoretic, and turbulent collections, AgI particles can activate cloud droplets as cloud condensation nuclei (CCN) through their soluble part from the burning of the seeding solution. The fraction of AgI acting as CCN is calculated by

$$F_{\text{ccn}} = 5(S_w - 1)^{1.5}, \tag{5}$$

where $S_w < 1.05$. Therefore, the maximum fraction of AgI particles acting as CCN is 5.6%.

All of these terms are limited by physically reasonable ranges such that 1) the summation of these terms cannot exceed unity; 2) deposition, condensation freezing, and CCN activation are limited by available vapor; and 3) contact freezing and immersion freezing are limited by available cloud droplets. Application of these formulas at temperature below 248 K is limited to their realizations at 248 K.

A point source of AgI particles is described by a release rate in kilograms per second and a grid point that indicates the source location. The locations can be fixed points in space to represent AgI generators on the ground, or they can dynamically change during simulation to represent moving sources, such as aircraft seeding. The AgI particles are assumed to have a single-mode lognormal distribution with a mean diameter of 0.04 μm (R. Stone 2012, personal communication) and a geometric standard deviation of 2 (Langer 1986; Meyers et al. 1995; Warburton et al. 1995b). Figure 1 illustrates the various interactions between AgI particles and hydrometeors in the coupled scheme. By tracking the conserved AgI number and mass within different hydrometeors, wet deposition of AgI is also calculated. The ingredients of the AgI seeding solution used by the WWMPP and the Idaho Power Company (IPC) are very similar to the solution tested by DeMott (1995).

3. Experimental setups

Although 2D simulations have difficulties in resolving the dynamics and energetics, such as the dispersion process and turbulence, as accurately as 3D simulations can, they are effective in isolating the contributions of individual physical processes and environmental factors to the phenomenon being simulated. Therefore, in this first paper we describe comprehensive 2D idealized sensitivity simulations and analyze the detailed microphysical and macrophysical processes associated with seeding to identify physical processes and environmental factors that are critical to the orographic cloud-seeding effects on the ground. We will then apply the process-level

TABLE 1. Summary of sensitivity experiments. The tested values of each parameter are indicated in boldface. Here, IN is the background ice nuclei concentration ratio relative to the default value that is calculated by the Cooper parameterization.

Case	T_{sfc} (K)	RH_{sfc}	z_m (m)	N_d (s^{-1})	U ($m\,s^{-1}$)	CN (cm^{-3})	IN	SR ($g\,h^{-1}$)
BASE	278.15	0.8	1500	0.011	15	100	1	20
T273	**273.15**	0.8	1500	0.011	15	100	1	20
T283	**283.15**	0.8	1500	0.011	15	100	1	20
RH70	278.15	**0.7**	1500	0.011	15	100	1	20
RH90	278.15	**0.9**	1500	0.011	15	100	1	20
Z1KM	278.15	0.8	**1000**	0.011	15	100	1	20
Z2KM	278.15	0.8	**2000**	0.011	15	100	1	20
N008	278.15	0.8	1500	**0.008**	15	100	1	20
N005	278.15	0.8	1500	**0.005**	15	100	1	20
U10	278.15	0.8	1500	0.011	**10**	100	1	20
U20	278.15	0.8	1500	0.011	**20**	100	1	20
CN300	278.15	0.8	1500	0.011	15	**300**	1	20
CN900	278.15	0.8	1500	0.011	15	**900**	1	20
IN001	278.15	0.8	1500	0.011	15	100	**0.01**	20
IN100	278.15	0.8	1500	0.011	15	100	**100**	20
SR02	278.15	0.8	1500	0.011	15	100	1	**4**
SR5	278.15	0.8	1500	0.011	15	100	1	**100**
SR1K	278.15	0.8	1500	0.011	15	100	1	**20 000**

understandings of cloud seeding that are described in this paper to interpret the results of 3D simulations of actual cloud-seeding cases in Xue et al. (2013, hereinafter Part II).

The model setups were similar to those of Xue et al. (2010, 2012). The 2D domain consisted of 421 grid points in the horizontal direction, with a grid spacing of 2 km. There were 61 terrain-following vertical levels in the domain, reaching the model top at 23 km. The vertical grid spacing varied from 20 m at the lowest layer to about 1400 m at the highest layer.[1] A Rayleigh-damping sponge layer was applied in the upper 10 km of the computational domain to minimize reflections of vertically propagating gravity waves from the rigid upper model boundary. A free-slip condition was imposed at the lower model boundary. An idealized bell-shaped mountain with peak height of 2000 m and half-width of 50 km was used to represent the scale of the Payette mountain region in Idaho. The mountain base is at 260 km on the upwind side, and the summit is at 400 km. A 1.5-order turbulent kinetic energy closure was used for turbulence. Monotonic flux limiters for advection of scalars and turbulence have been used in the simulations. The boundary layer parameterizations and the radiation schemes were switched off to simplify the model setup.

The sensitivity tests were constructed by running the model using different combinations of soundings (surface temperature T_{sfc}, relative humidity at the surface RH_{sfc}, the decay height of moisture z_m, dry Brunt–Väisälä frequency N_d, and horizontal wind U), and microphysical variables (cloud droplet number concentration CN and background ice nuclei number concentration IN). Airborne in situ measurements indicated that CN ranges from 20 to 400 cm^{-3} over the Medicine Bow area in Wyoming (Geerts et al. 2011) and from 50 to 500 cm^{-3} over the Payette region (B. Boe 2012, personal communication). Therefore, the default CN was set to 100 cm^{-3}, and two CN values of 300 and 900 cm^{-3} were tested in this study. To represent various background IN concentrations, a case with a very clean background (IN001) and a case with inferred dust storm (IN100) were simulated. The sensitivity cases being simulated are listed in Table 1.

The temperature profiles of the soundings are described by T_{sfc} and N_d. The profiles of the relative humidity are prescribed by the function

$$\mathrm{RH}(z) = \mathrm{RH}_{sfc} + \frac{\mathrm{RH}_{top} - \mathrm{RH}_{sfc}}{1 + \exp[-a(z - z_m)]}, \qquad (6)$$

where RH_{top} is relative humidity at the model top (set to 0.03), $a = 0.0015\,m^{-1}$ is the decay parameter, and z_m is in meters. The horizontal wind speed U is unidirectional, with a constant value below 10 km increasing linearly above that level to 40 $m\,s^{-1}$ at the top of the model. The idealized soundings have been used in many numerical studies focusing on interactions of wintertime orographic clouds and aerosols (Muhlbauer et al. 2010; Xue et al. 2010, 2012). They are representative

[1] The same number of grid points in the x direction, the same grid spacing, and the same vertical coordinate were used for the 3D simulations of real cases. See Part II for details.

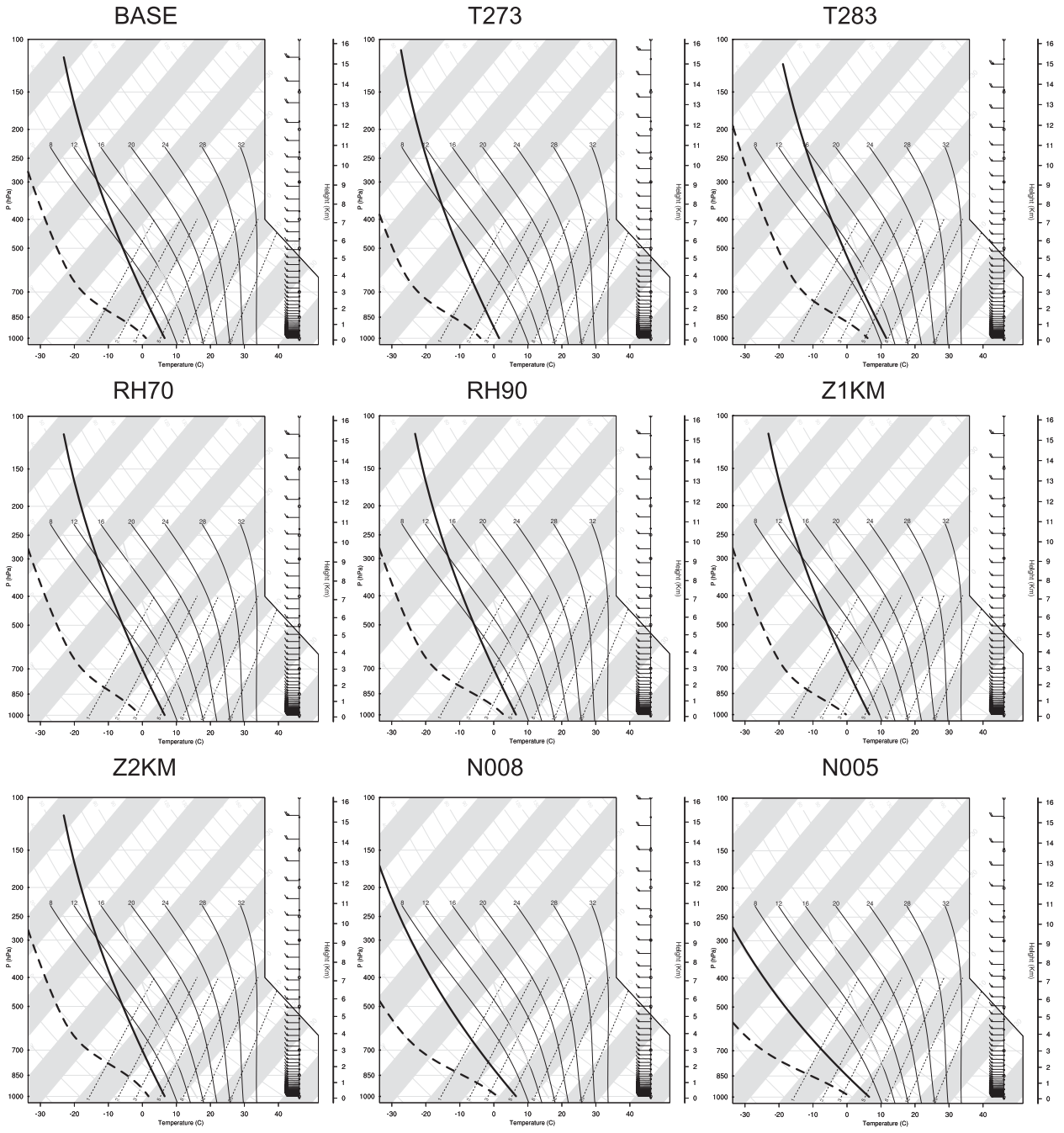

FIG. 2. Soundings for the BASE, T273, T283, RH70, RH90, Z1KM, Z2KM, N008, and N005 cases. The solid line is temperature (°C), and the dashed line is dewpoint temperature (°C).

of winter precipitating clouds and are suitable for the sensitivity tests in this study.

The soundings of the BASE, T273, T283, RH70, RH90, Z1KM, Z2KM, N008, and N005 cases are illustrated in Fig. 2. The soundings of the U10 and U20 cases are the same as the BASE case but with different wind speeds (not shown). The CN300, CN900, IN001, IN100, and seeding-rate (SR) cases use the same sounding as BASE. Among these soundings, RH70 and Z1KM have a slightly higher lifting condensation level (LCL) than the others because of their lower moisture content, and RH90 and Z2KM each have a lower LCL because of their higher moisture content. All soundings except the T273 and T283 cases show an LCL temperature of about −1°C. All

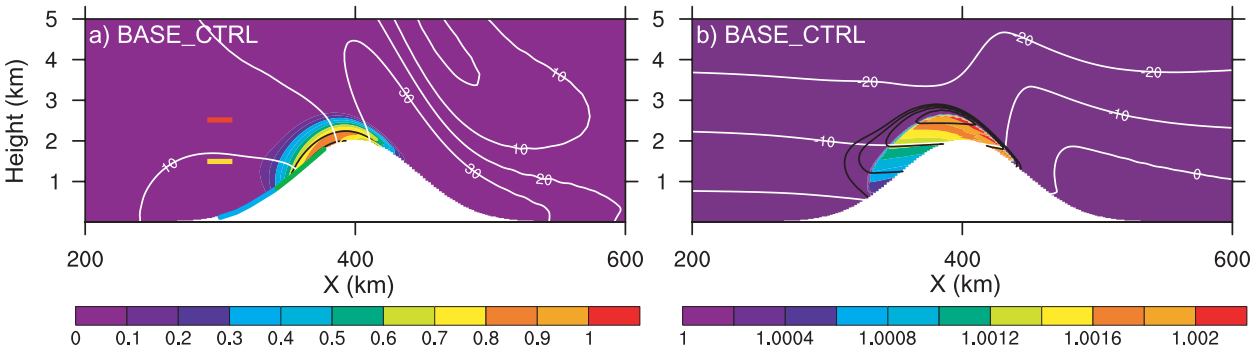

FIG. 3. Vertical cross section ($200 < X < 400$ km; $Z < 5$ km) of time-averaged fields between hour 2 and hour 6 in BASE_CTRL case for (a) cloud water mixing ratio (color shaded; g kg^{-1}), rainwater mixing ratio (black contours), snow mixing ratio (yellow contours at peak of topography; both the black and the yellow contours start at 0.01 g kg^{-1} with an interval of 0.1 g kg^{-1}), and horizontal wind speed (white contours, with an interval of 10 m s^{-1}) and (b) water saturation ratio (color shaded), ice saturation ratio (black contours, starting at 1 with an interval of 0.05), and temperature (white contours, with an interval of 10°C). The locations of lower-group ground generators, higher-group ground generators, lower flight track, and higher flight track are indicated by segments in blue, green, yellow, and red, respectively, in (a).

soundings except the N005 case generated well-defined orographic clouds (see details in section 4d).

For each set, one control case (CTRL) and four seeding cases (SEED) have been simulated for 10 h. Seeding occurred between hour 2 and hour 6 since the cloud reached steady state after 2 h. Among the four seeding cases, two are ground-based cases and two are airborne cases. For the ground-based seeding events, one group of five generators evenly distributed along the lower upwind slope between 300 and 340 km in the x axis (GL; blue segment in Fig. 3a) and another group of five generators along the higher upwind slope between 340 and 380 km (GH; green segment in Fig. 3a) were tested. In a similar way, flight tracks between 292 and 308 km at 1500 m MSL (AL) and at 2500 m MSL (AH) were tested as well (yellow and red segments in Fig. 3a). The default seeding rate was set to 20 g h^{-1} per generator, which is close to the actual seeding rate of the WWMPP and IPC seeding operations. The airborne seeding released the same amount of AgI as did the ground-based seeding. By using a bulk density of 1769 kg m^{-3} and a mean mass diameter of 0.0413 μm (R. Stone 2012, personal communication), an AgI number release rate of 8.5×10^{13} s^{-1} was calculated. In addition to the sensitivity of meteorological conditions, three seeding rates ($^1/_5$, 5, and 1000 times the default rate) have been used (respectively the SR02, SR5, and SR1K cases in Table 1) to test the sensitivity of seeding rates on seeding effects.

4. Results

The impacts of AgI seeding on precipitation and the microphysical pathways of orographic clouds are analyzed in detail in the following sections.

a. Base case

The Froude number Fr, which indicates the ratio of a fluid's inertia to buoyancy force, can be calculated by Fr $= U/(N_d H)$, where H is mountain height. For BASE cases, $U = 15$ m s^{-1}, $N_d = 0.011$ s^{-1}, and $H = 2000$ m, which yields Fr $= 0.682$ (i.e., a mountain wave is expected).

Figure 3a shows the time-averaged mixing ratios of all hydrometeor types and horizontal wind speed between hour 2 and hour 6 (seeding period) for the BASE_CTRL case in a subsection of the whole domain ($200 < X < 600$ km; $Z < 5$ km). During the seeding period, cloud water reached a steady-state value of 0.8 g kg^{-1}, rainwater was just above 0.1 g kg^{-1} and snow content was at 0.01 g kg^{-1}. The maximum liquid water content (LWC) simulated here was higher than previous observations over Wyoming (Geerts et al. 2011) and the Payette region (B. Boe 2012, personal communication) (0.2–0.3 g kg^{-1}), but the average simulated LWC (0.37 g kg^{-1}) was still close to observations (see section 5 for details). As mentioned before, these 2D idealized simulations focused on the physical processes that are associated with seeding and not on reproducing the real events. Ice crystals and graupel particles were not apparent in the cloud. A typical mountain wave with reduced wind speed in the lower part of the windward slope and an accelerated stream on the lee side was observed. The cloud base was located at about 700 m, and the cloud top reached 2600 m.

The time-averaged saturation ratios over water and ice and averaged temperature over the same time period are illustrated in Fig. 3b for the BASE_CTRL case. The cloud-base temperature was 0°C, and the cloud-top temperature was about −15°C. Since the activation rates

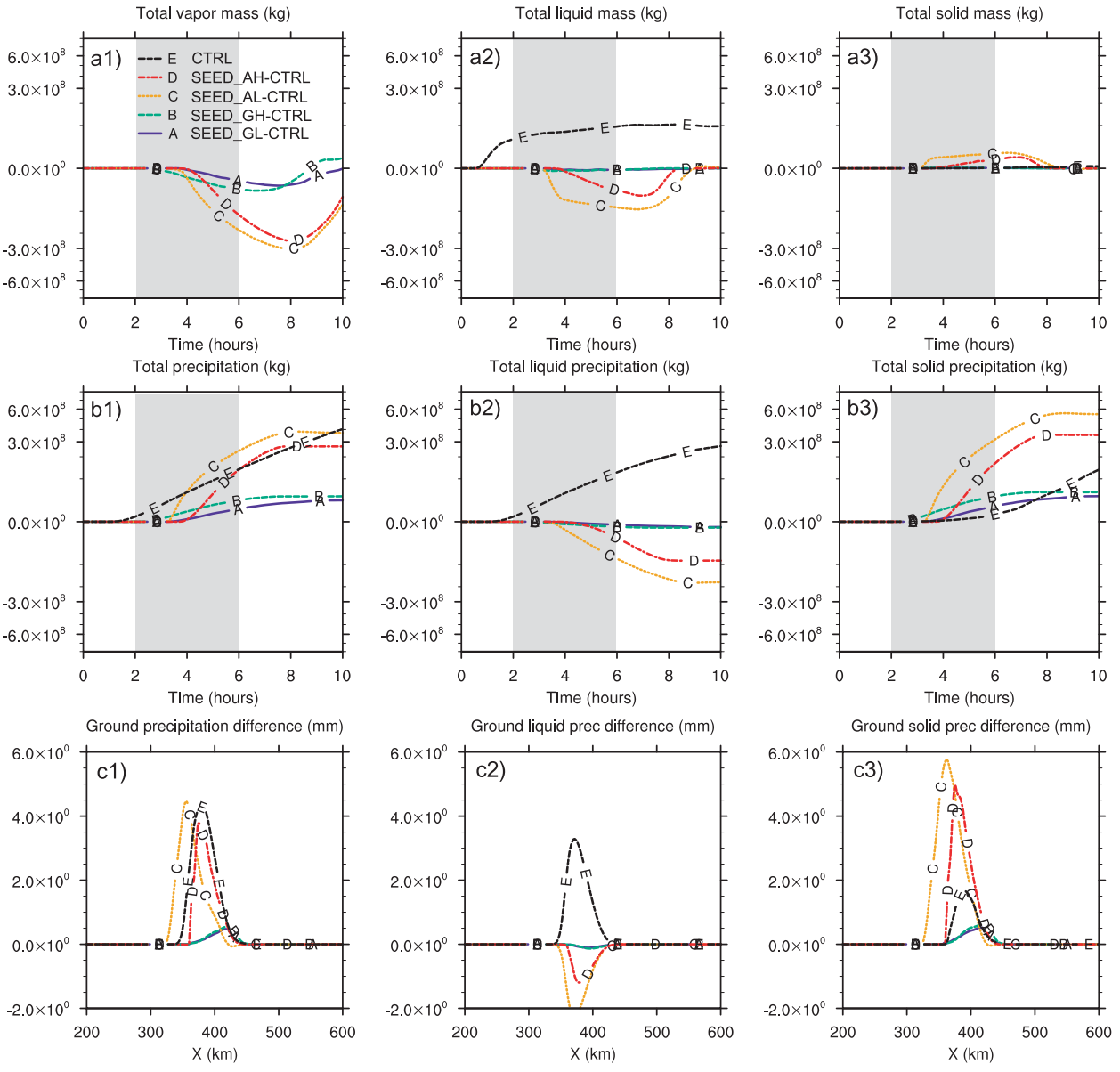

FIG. 4. Time series of (a1) total vapor mass (kg), (a2) total liquid water mass (kg), (a3) total ice-phase water mass (kg), (b1) total precipitation (kg), (b2) total liquid precipitation (kg), and (b3) total ice-phase precipitation (kg) and spatial distribution of (c1) total precipitation (mm), (c2) total liquid precipitation (mm), and (c3) total ice-phase precipitation (mm). Curves A–D indicate differences between BASE_SEED_GL, BASE_SEED_GH, BASE_SEED_AL, and BASE_SEED_AH and BASE_CTRL, respectively. Curve E represents the value of the BASE_CTRL case. The total vapor mass of BASE_CTRL is around 8.3×10^9 kg for the entire period, which is not shown in (a1). The vertical axis in (a1)–(a3) and (b1)–(b3) is nonlinear, with each tick mark representing 1×10^8 kg. The seeding period is indicated by the gray area in each time-series plot.

of all four modes of AgI are functions of saturation ratios over water/ice and/or temperature (see section 2), the average distributions of these fields over the seeding period can be used to estimate AgI activation ratio and seeding effect.

All seeding cases—ground based and airborne—depleted more vapor mass than did the CTRL case, although the instant value of the BASE_SEED_GH case was higher than BASE_CTRL after 8 h (Fig. 4a1). All seeding cases also generated more total precipitation (rain, snow, and graupel) and ice-phase precipitation (snow and graupel) on the ground than did the CTRL case (Figs. 4b1, 4b3, 4c1, and 4c3). Airborne seeding (curves C and D) consumed more vapor and liquid water in the cloud than did ground-based seeding (curves A and B), which led to more ice-phase hydrometeors in

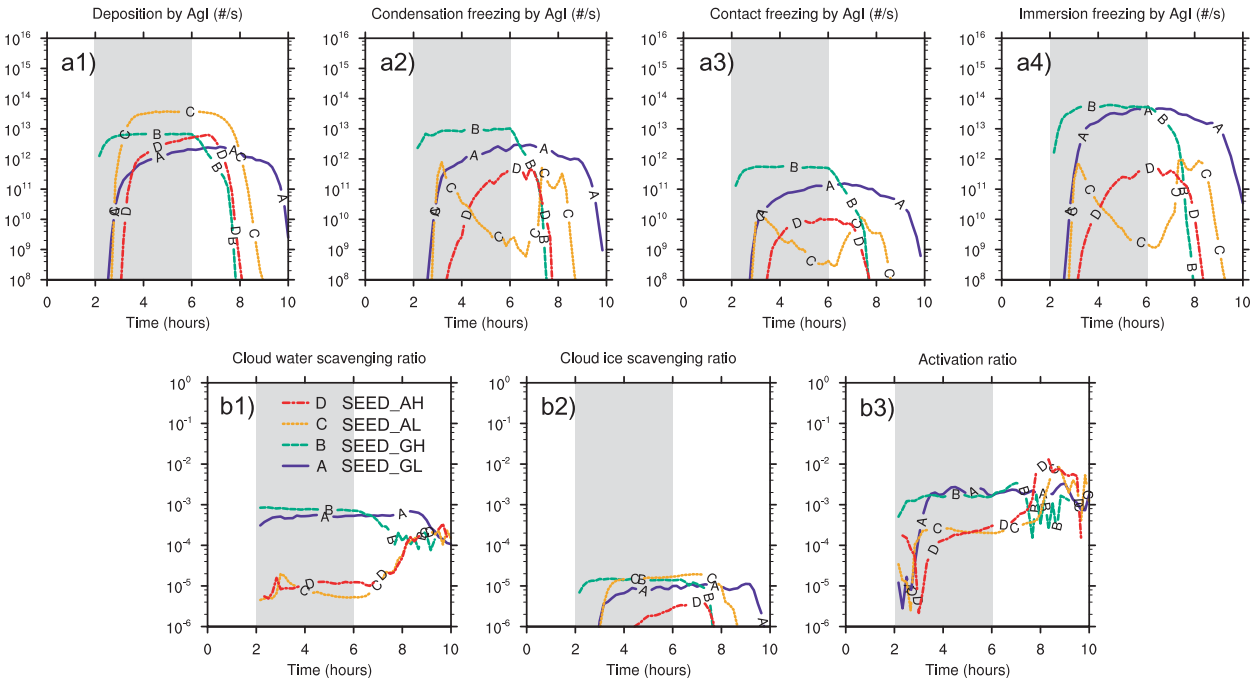

FIG. 5. Time series of AgI activation rate (s^{-1}) for (a1) deposition, (a2) condensation freezing, (a3) contact freezing, and (a4) immersion freezing, and time series of (b1) AgI scavenging ratio by cloud water, (b2) AgI scavenging ratio by cloud ice and (b3) AgI activation ratio. Curves A–D indicate BASE_SEED_GL, BASE_SEED_GH, BASE_SEED_AL, and BASE_SEED_AH, respectively. All variables are in logarithmic scale. The seeding period is indicated by the gray area in each plot.

the cloud, less liquid precipitation, and more ice-phase precipitation on the ground (Fig. 4). Under the stable stratified condition of the BASE sounding and smooth topography, AgI particles released by ground generators stayed close to the ground, whereas AgI particles released from aircraft flew along the streamline with minimum dispersion and entered the cloud well above the cloud base. Therefore, ice crystals nucleated by AgI particles from airborne seeding cases had more time to grow through diffusion and riming processes than did those nucleated by AgI from ground generators. AgI particles from the lower flight track (curve C) experienced more growth time than those from the higher flight track (curve D).[2] Thus, the seeding effect (i.e., total precipitation enhancement) of the BASE_SEED_AL case was greater than that of the BASE_SEED_AH case (Fig. 4b1). At the surface, seeding effects from the airborne seeding case occurred about an hour after seeding (Figs. 4b1 and 4c1), which is in good agreement with previous observations (Deshler et al. 1990).

Figures 5a1–5a4 show the time series of AgI nucleation rates (s^{-1}) of four modes over the entire domain for all seeding cases. Deposition was the dominant mode for airborne seeding, whereas immersion freezing dominated in ground-based seeding cases. Contact freezing was the weakest among all four modes for both ground-based and airborne seeding cases. The difference of roughly two orders of magnitude between condensation-freezing and contact-freezing modes simulated here agrees with the results simulated by Li and Pitter (1997) in which the cloud droplet concentration was similar to the value used in this study. For airborne seeding cases, AgI particles entered ice-supersaturated regions before reaching the liquid water cloud (see Fig. 3b). Therefore, AgI particles acted solely as deposition nuclei at this time. Although deposition was identified as a slow and ineffective mode of AgI nucleation (DeMott 1995), the absence of liquid water and collocation of high ice supersaturation and low temperature made this mode important in this case. These nucleated ice crystals upwind of the orographic cloud experienced a longer time of diffusional growth than those nucleated through other modes, which led to the majority of the precipitation enhancement on the ground. For ground-based seeding cases, AgI particles were directly emitted into the water-supersaturated region of the cloud, which facilitates condensation freezing and immersion freezing through CCN activation of AgI particles. Although AgI particles from

[2] The cloud region at an altitude of 1500 m was broader than that at 2500 m, as seen in Fig. 3.

ground generators entered regions of higher ice supersaturation than in airborne cases, the warmer temperature close to the ground made the deposition activation rate of ground-based seeding lower than that of airborne seeding [see Eq. (1)].

Contact freezing has been identified as a dominant mode of AgI under low temperatures by laboratory and numerical studies (DeMott 1995; Meyers et al. 1995). Observational and some numerical studies indicated that contact freezing is not the major nucleation mechanism contributing to seeding effects, however (Deshler and Reynolds 1990; Chai et al. 1993; Li and Pitter 1997). Since contact freezing is a function of F_{scav} [Eq. (3)] and F_{scav} is a function of hydrometeor concentration and AgI particle concentration, a low cloud droplet concentration limits the importance of this mode (Li and Pitter 1997).[3] Laboratory and numerical studies demonstrated that immersion freezing is a slow and unimportant mode of AgI (Pitter and Pruppacher 1973; Meyers et al. 1995); the insignificant contribution of this mode was calculated for hydrophobic AgI particles (Meyers et al. 1995), however. Immersion freezing can be important when AgI particles act as CCN. AgI particles enter cloud droplets through scavenging and activation processes when contact freezing is weak. Such AgI-containing cloud droplets will be nucleated by immersion freezing when they encounter regions with favorable conditions (low temperatures). The much higher nucleation rate of immersion freezing than of contact freezing in this study was attributed to two limitations that are related to the Thompson scheme and the two-dimensional model setup. First, the cloud droplet concentration was a fixed value ($100\,\text{cm}^{-3}$) everywhere throughout the simulation. Under such a condition, newly activated AgI particles did not increase the cloud droplet concentration, which artificially suppressed the contact-freezing mode. Second, the weak dispersion and turbulence simulated by the 2D domain resulted in an unrealistically high concentration of AgI particles, especially in ground-based seeding cases. Since contact freezing was weak, most of the scavenged AgI particles stayed inside the cloud droplet as inactive nuclei. The continuous scavenging of high concentration of AgI particles by cloud droplets led to very high F_{imm} values [see Eq. (4)]. When these cloud droplets with high F_{imm} moved into regions with low temperatures, immersion freezing became dominant. Additional seeding experiments that assumed no ability of AgI particles to serve as CCN showed that the immersion-freezing activity was reduced while contact freezing was more active. The nucleation rate of immersion freezing was still about an order of magnitude higher than that of contact freezing, however, because of the model artifacts.

Figures 5b1 and 5b2 illustrate the time series of the ratios of AgI particles scavenged by cloud water and ice, respectively, through Brownian, phoretic, and turbulent mechanisms for all seeding cases. The higher cloud water scavenging ratios of ground-based seeding cases were the result of higher AgI concentrations close to the ground than those of airborne cases (about two orders of magnitude higher). The high ice scavenging ratio in the BASE_SEED_AL case was caused by high ice crystal concentrations realized through the deposition nucleation process (Fig. 5a1). The local AgI activation ratio, defined as the number of AgI particles that nucleate ice crystals through four modes to the number of AgI particles in the places where nucleation of these particles occurs, is plotted in Fig. 5b3. Since deposition and condensation freezing are not related to the scavenging process, the activation ratio can be higher than the scavenging ratio. Ground-based seeding cases had higher activation ratios because of their higher scavenging ratios than did airborne seeding cases. The noisy signals in the time series plots after hour 7 were related to the interactions between low concentrations of AgI particles and the downwind edge of the cloud (most of the AgI had been advected downwind of the cloud after this time). Since both water and ice supersaturation ratios reached high values in this region (Fig. 3b), the high local activation ratio is expected. It is found that, in general, about 0.2% of the AgI particles acted as active ice nuclei in ground-based seeding cases and that the ratio was about 0.02%–2% in airborne seeding cases under BASE conditions. The average ice crystal number concentration ranged from 35 (GL, GH, and AH) to $90\,\text{L}^{-1}$ (AL) for seeding cases, which is in good agreement with the findings of Deshler et al. (1990), Meyers et al. (1995) and Geerts et al. (2010).

Through altering the microphysical pathways and cloud macrophysical properties, AgI particles modified the precipitation amount, phase, and spatial distribution on the ground. Table 2 lists the total precipitation (mm), snow ratio defined as snow amount to total precipitation (%), precipitation difference between the seeding and the control case (mm), relative change of precipitation between the seeding and the control case (%), and spillover ratio, defined as leeward accumulated precipitation to total precipitation (%), for the BASE experiments. The ground-based seeding cases increased precipitation by 10%, which is in agreement with previous studies (Givati and Rosenfeld 2005; Manton and Warren 2011). Ground seeding did not modify the

[3] Note that the cloud droplet concentration was 2100–4300 cm^{-3} in DeMott (1995) and was only $100\,\text{cm}^{-3}$ in Li and Pitter (1997).

TABLE 2. Precipitation features of the BASE experiments. Here, P is total precipitation on the ground, including both water and ice phases; R_{snow} is snow ratio, defined as snow amount to total precipitation; and SPR is spillover ratio, defined as leeward accumulated precipitation to total precipitation.

Case	P (mm)	R_{snow} (%)	$P - P_{ctrl}$ (mm)	$(P - P_{ctrl})/P_{ctrl}$ (%)	SPR (%)
CTRL	101	34	0.0	0.0	17
SEED_GL	111	41	10	10	22
SEED_GH	113	42	12	12	23
SEED_AL	194	88	93	92	11
SEED_AH	167	73	67	66	18

snow ratio much. Airborne seeding cases significantly increased the precipitation (more than 66%) and dramatically increased the snow ratio. It is hard to compare the simulated airborne seeding effects with observations since Deshler et al. (1990) pointed out that the existing precipitation network was not enough to resolve the airborne seeding effects. The AgI particles from ground generators stayed close to the surface over the smooth idealized topography. Therefore, the ice crystals nucleated by these AgI particles had little time to grow through diffusion and riming, which resulted in small snow enhancement. Under real complex-terrain conditions, however, the terrain-induced vertical motions can loft generator-emitted AgI particles to relatively high altitudes (see Part II for details). On the other hand, aircraft-released AgI entered the cloud well above the cloud base, and the ice crystals nucleated by deposition of AgI grew through both the Bergeron–Findeisen process and the riming process prior to their falling to the ground. Thus, much of the rainwater was depleted and much more snow precipitated to the ground in airborne cases (see Figs. 4b2, 4b3, 4c2, and 4c3).

The spatial distributions of enhanced precipitation due to seeding were very different for ground-based and airborne seeding. Ground seeding mainly enhanced the precipitation on the lee side [high spillover ratio (SPR) in Table 2 and Fig. 4c1], which is associated with high water supersaturation[4] and slow terminal velocity of the AgI-nucleated crystals. Most of the precipitation enhancement was located on the windward side for the lower-flight-track airborne case (low SPR of SEED_AL in Table 2 and Fig. 4c1) because of the high ice supersaturation, abundant cloud water content, and fast terminal velocity of large rimed particles over this region (see Fig. 3b).[5] The simulated upwind seeding effect of the SEED_AL case was observed by Deshler et al. (1990). For the higher-flight-track airborne seeding case (SEED_AH), AgI particles at the higher altitude experienced higher ice supersaturation but less water content and smaller cloudy area than for the SEED_AL case. Thus, the nucleated ice crystals had a slower growth rate than in the SEED_AL case. Therefore, snow in the SEED_AH case reached the ground later than in the SEED_AL case, causing the SPR to be slightly higher than in the CTRL case (see Fig. 4c3).

The analyses in this section explored the microphysical pathways that AgI particles took in modifying the cloud macrophysical features and precipitation properties in a typical orographic cloud. In the following sections, we mainly focus on how different meteorological conditions and microphysical characteristics affect changes in precipitation that are due to seeding.

b. Temperature effects

The sensitivity of seeding effects to temperature (±5°C from the BASE conditions) is described in this section. Figure 6, in the same format as Fig. 3, shows distributions of the various fields for the T273_CTRL and T283_CTRL cases. For the T273_CTRL case, lower cloud water mixing ratio ($0.6\,g\,kg^{-1}$), lower rainwater mixing ratio ($\sim 0.01\,g\,kg^{-1}$), and higher snow mixing ratio ($>0.11\,g\,kg^{-1}$) than for the BASE_CTRL case were observed (see Fig. 6a1 and Fig. 3a). When the surface temperature was 5°C lower than the BASE case, the cloud-base and cloud-top temperatures were lowered by 5°C (Fig. 6b1). Although the water-supersaturated region of T273_CTRL was very similar to that of BASE_CTRL, the T273_CTRL case generated broader areas and higher values of ice supersaturation than did the BASE_CTRL case (Fig. 6b1). When compared with T273_CTRL, the T283_CTRL case had the opposite trend relative to the BASE_CTRL case. Higher cloud water ($0.9\,g\,kg^{-1}$), higher rainwater ($>0.21\,g\,kg^{-1}$), lower snow mixing ratio ($<0.01\,g\,kg^{-1}$), warmer cloud-base and cloud-top temperatures, and smaller ice-supersaturated areas than in the BASE_CTRL case were simulated (Figs. 6a2 and 6b2).

The same precipitation features as described in Table 2 for the BASE experiments are listed in Table 3 for the T273 and T283 experiments. T273_CTRL generated slightly more total precipitation and a much higher snow ratio than did the BASE_CTRL case because of its colder temperature and thus more efficient ice-related microphysical processes (Li and Pitter 1997). Under such conditions, ground-based seeding cases had effects [$P - P_{ctrl}$, $(P - P_{ctrl})/P_{ctrl}$, and SPR] that were very similar to those of the BASE ground-based seeding cases (see Tables 2 and 3) for the same reasons mentioned in

[4] High water supersaturation facilitates condensation-freezing and immersion-freezing processes.

[5] High ice supersaturation and high water content facilitate deposition, contact-freezing, Bergeron–Findeisen, and riming processes.

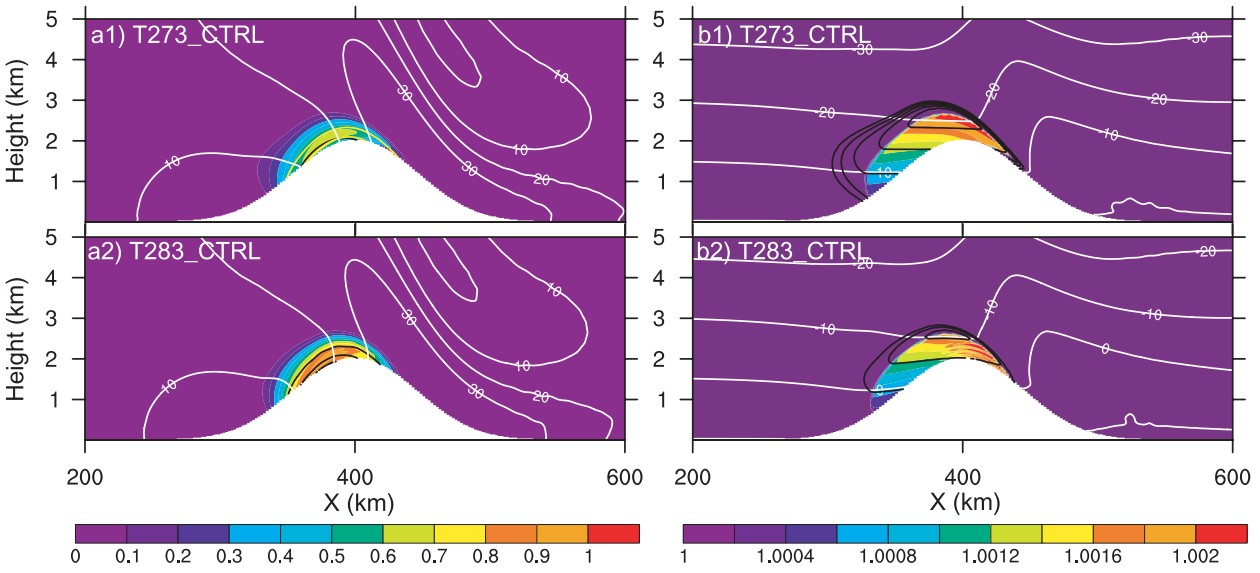

FIG. 6. As in Fig. 3, but for (a1),(b1) T273_CTRL and (a2),(b2) T283_CTRL.

the previous section. Because of the low liquid water content in the cloud, however, the Bergeron–Findeisen process and the riming process of airborne seeding cases were not as active as in BASE airborne seeding cases. As a result, the precipitation enhancements from airborne seeding in the T273 experiments were reduced relative to those of BASE (see Tables 2 and 3). The SPR values of the airborne seeding cases were also similar to those of the BASE cases because of their similar cloud structure, microphysical pathways, and wind fields.

When the surface temperature was 283 K, all natural precipitation was in the liquid phase. The efficient warm-rain processes of T283_CTRL generated more precipitation on the ground and lower SPR than in the BASE_CTRL case. Since AgI particles from ground generators remained very close to the ground and, in this case, the temperature close to the ground was almost always higher than the AgI activation threshold, the ground-based seeding cases of T283 experiments produced negligible precipitation enhancements and SPR changes (Table 3). Reisin et al. (1996) also found that seeding effects in warm clouds were negligible relative to cold clouds, but in the convective regime. On the other hand, the overlap of ice-supersaturated regions and regions of high liquid water content, combined with sufficiently low temperature in the cloud, guaranteed efficient AgI nucleations, the Bergeron–Findeisen process, and the riming process in the airborne seeding cases of the T283 experiments (see Fig. 6b2). Therefore, the T283 airborne seeding cases achieved similar seeding effects (similar precipitation enhancements and SPR but slightly lower relative precipitation enhancements) in comparison with the BASE airborne seeding cases (see Tables 2 and 3).

This group of sensitivity experiments indicates that there exists an optimum temperature condition (T_{sfc} = 278 K in this case) under which the absolute and the relative precipitation enhancements are maximized. Furthermore, when the surface temperature is high, ground-base seeding is ineffective but airborne seeding can still be very effective, which is important information for seeding operations.

c. *Humidity effects*

The sensitivity of seeding effects to humidity was investigated through two groups of experiments. One group

TABLE 3. As in Table 2, but for T273 and T283.

Case	P (mm)		R_{snow} (%)		$P - P_{ctrl}$ (mm)		$(P - P_{ctrl})/P_{ctrl}$ (%)		SPR (%)	
	T273	T283	T273	T283	T273	T283	T273	T283	T273	T283
CTRL	107	121	90	0.0	0.0	0.0	0.0	0.0	17	11
SEED_GL	117	121	92	0.0	10	0.4	9.6	0.3	18	11
SEED_GH	119	121	93	0.0	12	0.4	11	0.3	20	11
SEED_AL	175	213	97	72	68	92	64	76	11	11
SEED_AH	163	163	95	36	56	42	52	35	16	18

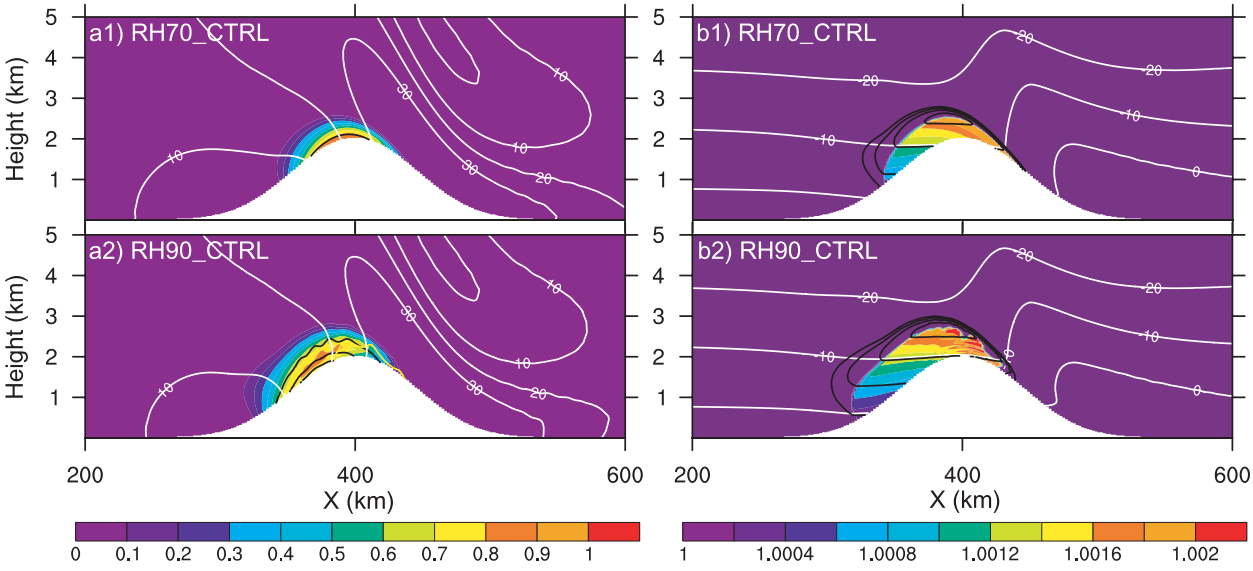

FIG. 7. As in Fig. 3, but for (a1),(b1) RH70_CTRL and (a2),(b2) RH90_CTRL.

examined the effect of differing surface relative humidities (RH70 and RH90) that represented different surface conditions and latent heat fluxes. As illustrated in Figs. 7a1 and 7a2, lower surface humidity formed a shallower and less extensive orographic cloud whereas higher surface humidity generated a deeper and broader orographic cloud than in the BASE_CTRL case. Although the maximum cloud water mixing ratios of these two cases were similar to that of BASE_CTRL, the rain and snow mixing ratios were smaller in RH70_CTRL and greater in RH90_CTRL. The water and ice-supersaturated areas were correspondingly smaller in the RH70_CTRL case and broader in the RH90_CTRL case (Figs. 7b1 and 7b2).

As a result of less available water vapor (humidity), the RH70_CTRL case generated less precipitation than did BASE_CTRL whereas RH90_CTRL generated more (Table 4). Through similar mechanisms of how AgI particles affect precipitation in the BASE experiments, both ground-based and airborne seeding techniques produced similar precipitation enhancements and SPR trends in the RH70 and RH90 experiments (Table 4). In a relative sense, however, precipitation enhancements were higher in all RH70 seeding cases and lower in RH90 seeding cases when compared with BASE seeding cases.

The other group of experiments that examined the effect of humidity on seeding varied the depth of the moisture layer (Z1KM and Z2KM) that represents the depth of synoptic-scale advection of moisture. As shown in Figs. 7 and 8, the cloud macrophysical properties of the Z1KM_CTRL and the Z2KM_CTRL cases were very similar to those of the RH70_CTRL and the RH90_CTRL cases, respectively. A shallower moisture layer generated a shallower and less extensive orographic cloud, and vice versa for the deeper moisture layer case. Therefore, the precipitation features of these two cases resembled those of RH70 and RH90 closely (Table 5). Close investigation shows that the Z2KM_CTRL case generated more snow, which resulted in smaller seeding effects and SPR than in the RH90_CTRL case. The very little precipitation enhancement of the Z1KM_SEED_AH case was the result of the fact that the cloud top of the Z1KM cases was lower than 2500 m and thus the AgI particles released from the higher flight track (2500 m) barely impacted the cloud.

TABLE 4. As in Table 2, but for RH70 and RH90.

	P (mm)		R_{snow} (%)		$P - P_{ctrl}$ (mm)		$(P - P_{ctrl})/P_{ctrl}$ (%)		SPR (%)	
Case	RH70	RH90	RH70	RH90	RH70	RH90	RH70	RH90	RH70	RH90
CTRL	37	198	30	35	0.0	0.0	0.0	0.0	24	17
SEED_GL	53	210	57	42	17	12	45	6.2	36	20
SEED_GH	53	214	57	43	16	16	45	7.9	36	21
SEED_AL	121	296	93	85	85	98	232	50	12	14
SEED_AH	79	270	76	67	43	72	117	36	28	15

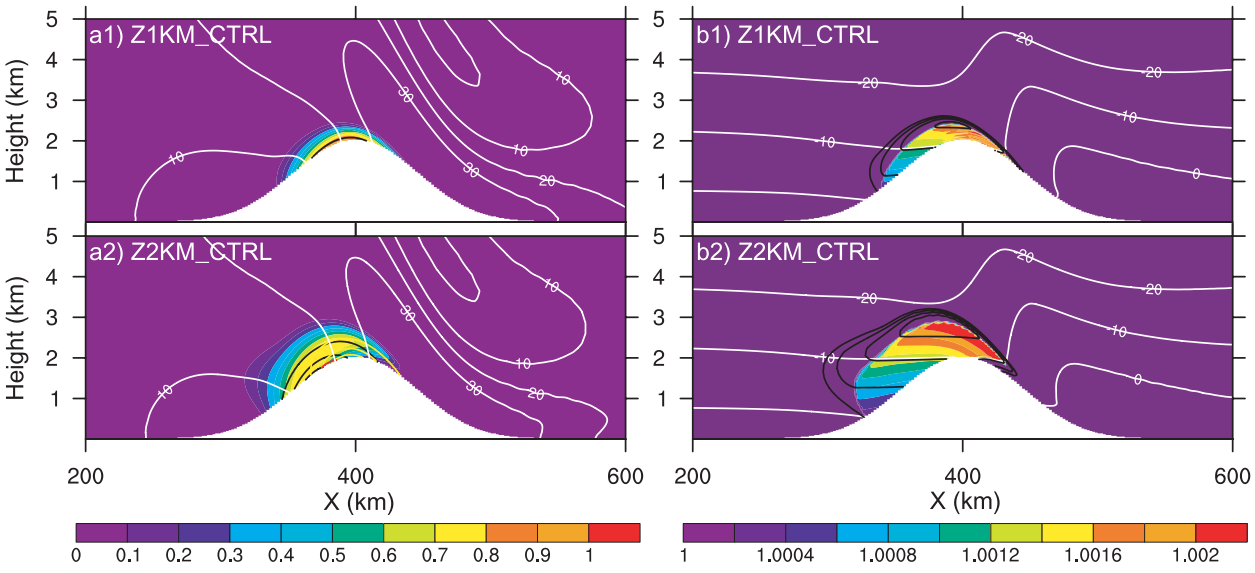

FIG. 8. As in Fig. 3, but for (a1),(b1) Z1KM_CTRL and (a2),(b2) Z2KM_CTRL.

For the Z2KM_SEED_AH case, the cloud top was well above 2500 m at around 3000 m. Therefore, AgI-nucleated ice crystals experienced similar growth time as in the Z2KM_SEED_AL case through both diffusion and riming and therefore produced precipitation enhancement and SPR that were similar to those in the Z2KM_SEED_AL case (Table 5).

d. Stability and wind speed effects

In this section, the sensitivities of seeding effects to atmospheric stability (lower values of N_d) and wind speed (higher and lower values of U) are examined. Unlike with the previous experiments investigating the effects of varying temperature and humidity, the dynamical features of these experiments were different from those of the BASE experiments. As seen in Figs. 9a1 and 9b1, the structure of the orographic cloud in the N008_CTRL case was not as well defined as those of previous experiments (Figs. 3, 6, 7, and 8). As compared with these conditions (Fr = 0.938), the Froude number became 1.5 in the N005_CTRL case and the moist flow with such a high Fr became very unstable and convective (see Figs. 2 and 9a2). No ground-attached orographic cloud was observed in the N005_CTRL case (Figs. 9a2 and 9b2).

When the atmosphere was slightly less stable than it is in the BASE case, the N008_CTRL case (see Fig. 2) generated more precipitation than the BASE_CTRL case (Table 6). Because the cloud was unstable and slightly convective, the AgI particles from ground generators were transported to higher altitudes relative to the BASE ground-based seeding cases. Thus, higher precipitation enhancements were observed in the N008 ground-based seeding cases. When the atmosphere was much less stable than the BASE case (such as N005), however, the moist flow completely turned into a convective regime. Under such conditions, there was little liquid water in the cloud and the ice-phase microphysical processes were very active. Even though the AgI particles were transported to higher altitudes, natural ice production was very efficient at this altitude and there was not much available vapor to nucleate the AgI particles, which led to marginal precipitation enhancements and negligible SPR changes in the N005 seeding cases. The ~10% precipitation enhancements for all seeding scenarios in N005 compared quantitatively well to the

TABLE 5. As in Table 2, but for Z1KM and Z2KM.

Case	P (mm)		R_{snow} (%)		$P - P_{ctrl}$ (mm)		$(P - P_{ctrl})/P_{ctrl}$ (%)		SPR (%)	
	Z1KM	Z2KM	Z1KM	Z2KM	Z1KM	Z2KM	Z1KM	Z2KM	Z1KM	Z2KM
CTRL	27	225	7.4	65	0.0	0.0	0.0	0.0	21	14
SEED_GL	62	227	71	67	35	2.3	132	1.0	47	14
SEED_GH	59	228	68	66	32	3.2	122	1.4	45	14
SEED_AL	97	305	90	90	70	79	265	35	13	10
SEED_AH	33	305	27	88	6.4	80	24	35	33	11

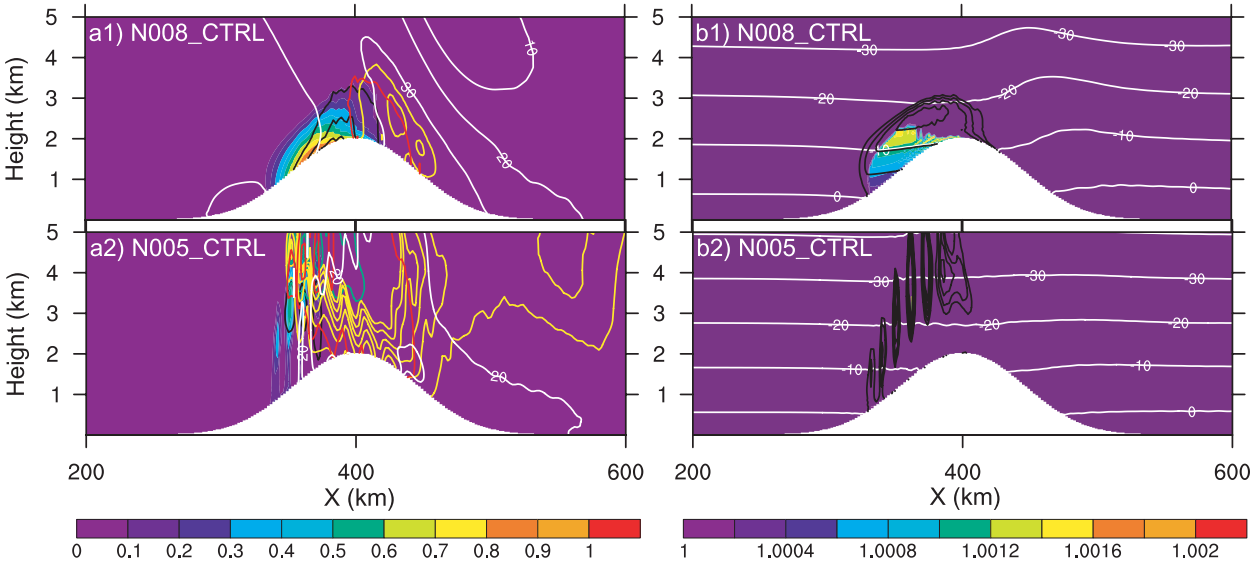

FIG. 9. As in Fig. 3, but for (a1),(b1) N008_CTRL and (a2),(b2) N005_CTRL. The green and red contours in (a1) and (a2) indicate mixing ratios of ice and graupel, respectively, starting at 0.001 g kg^{-1} with an interval of 0.01 g kg^{-1}.

results of previous numerical simulations of seeding effects on convective clouds (Reisin et al. 1996; Curic et al. 2007).

When the wind speed was reduced from 15 to 10 m s^{-1} (U10), the Froude number became 0.455. Laboratory experiments and theory predict that the flow is blocked at low levels of a 2D barrier when Fr $<$ 0.5 (Baines 1995). This is evident in Fig. 10a1, which shows that the wind close to the ground between 300 and 340 km was reversed. The slower wind speed also produced a shallower and less extensive orographic cloud relative to cases with $U = 15\,\mathrm{m\,s^{-1}}$ (Figs. 10a1 and 10b1). When $U = 20\,\mathrm{m\,s^{-1}}$, the Froude number increased to 0.909. As expected, a deeper and broader orographic cloud was formed under the stronger wind conditions (Figs. 10a2 and 10b2).

The U10_CTRL case generated the least amount of precipitation on the ground among all CTRL simulations (11 mm as listed in Table 7), and the U20_CTRL case generated the second highest amount of total precipitation (201 mm), which agreed with Li and Pitter (1997). Thus, natural precipitation processes are very sensitive to wind speed, with all other conditions being the same. Since AgI-nucleated ice crystals had a longer growth time for the U10 experiments than for the BASE seeding cases, very high relative precipitation enhancements were achieved (Table 7). On the other hand, these ice crystals had less growth time in the U20 seeding cases, and hence lower relative precipitation enhancements were observed (Table 7). Similar to the Z1KM_SEED_AH and the RH70_SEED_AH cases, the U10_SEED_AH case showed weaker impacts on precipitation because of the low cloud top. The impacts on SPR by seeding were similar to those of the BASE experiments for both U10 and U20.

In the U10 experiments, the flow at the lower level was blocked by the mountain (Fig. 10a1). Because the cloud base was low enough to incorporate AgI particles from the lower group of ground generators, seeding effects were observed. Additional experiments using the sounding of Z1KM with a wind speed of 10 m s^{-1} revealed that AgI particles from the lower group of ground generators could not reach the cloud and thus no seeding effects were simulated, whereas GH seeding cases

TABLE 6. As in Table 2, but for N008 and N005.

Case	P (mm)		R_{snow} (%)		$P - P_{ctrl}$ (mm)		$(P - P_{ctrl})/P_{ctrl}$ (%)		SPR (%)	
	N008	N005	N008	N005	N008	N005	N008	N005	N008	N005
CTRL	166	57	21	84	0.0	0.0	0.0	0.0	34	74
SEED_GL	198	62	62	85	32	5.4	19	9.5	37	71
SEED_GH	190	60	56	85	23	3.1	14	5.5	36	72
SEED_AL	236	62	76	85	70	5.7	42	10	21	71
SEED_AH	202	62	48	85	35	5.4	21	9.5	45	71

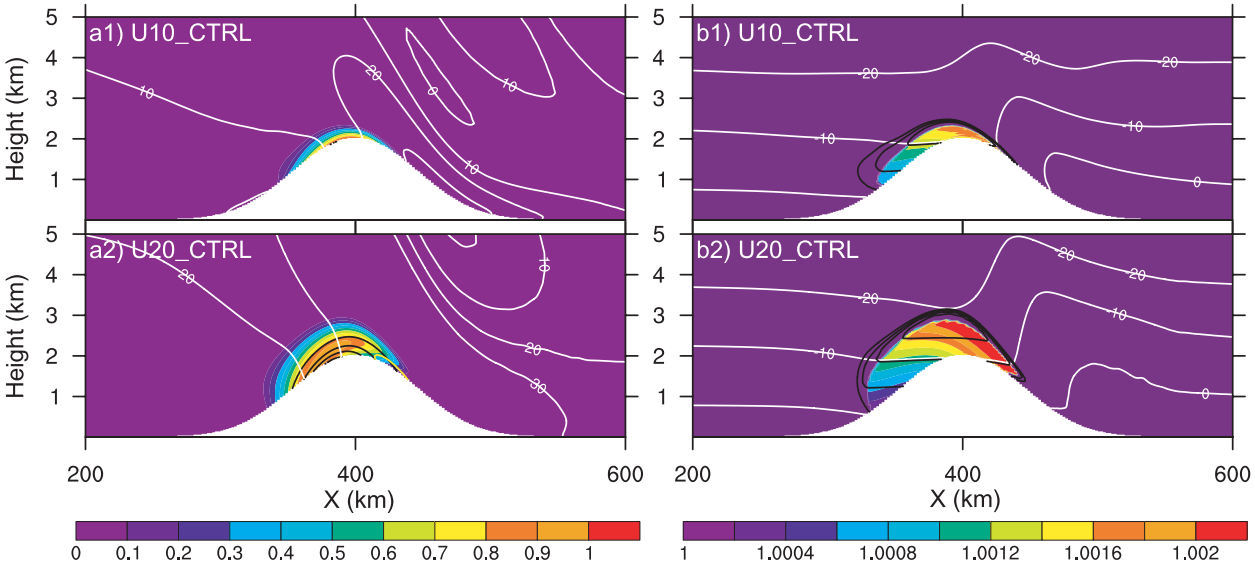

FIG. 10. As in Fig. 3, but for (a1),(b1) U10_CTRL and (a2),(b2) U20_CTRL.

still showed enhanced precipitation under such conditions. This result indicates that blocking conditions should be considered in the placement of seeding generators, as well as in seeding operations, so that the most effective group of generators is turned on.

e. *Cloud microphysics effects*

Having investigated the impacts of varying meteorological conditions on seeding effects, we focus in this section on the impacts that cloud microphysical properties have on seeding effects. The variables tested were cloud droplet number concentrations, indicative of pollution levels in the atmosphere, and background ice nuclei concentrations representing conditions ranging from a very clean background to dust storms. The Thompson microphysics scheme uses a modified version of the Cooper parameterization (Cooper 1986) to calculate how many IN are active under certain temperatures. The IN values in the IN001 and IN100 experiments were realized by multiplying the IN concentration from that of the Cooper parameterization by 0.01 and 100 to represent extremely clean and dust-storm conditions. All of the CN and IN cases used the same sounding as did the BASE experiment.

As the pollution level (CN) increased, the cloud water mixing ratio increased because of the suppression of the collision–coalescence (C–C) process. The maximum cloud mixing ratios of the CN300_CTRL and the CN900_CTRL cases during hour 2 and hour 6 (the seeding period) reached 0.9 and 1.0 g kg^{-1}, respectively (not shown). At the same time, rain mixing ratios were reduced to 0.01 and less than 0.01 g kg^{-1}, respectively (not shown). Since the AgI scavenging processes are functions of hydrometeor concentrations, higher scavenging ratios of AgI particles by polluted clouds are expected, and indeed they are demonstrated in Figs. 11a1 and 11a2 in which the maximum scavenging ratio exceeded 0.3%. The local AgI activation ratios increased with the increasing scavenging rates in ground-based seeding cases, as shown in Figs. 11b1 and 11b2 in which the maximum local activation ratio exceeded 1%. This is because immersion freezing is the most important nucleation mode, as demonstrated previously in section 4a (also see Fig. 5b3). The dominant nucleation

TABLE 7. As in Table 2, but for U10 and U20.

	P (mm)		R_{snow} (%)		$P - P_{ctrl}$ (mm)		$(P - P_{ctrl})/P_{ctrl}$ (%)		SPR (%)	
Case	U10	U20	U10	U20	U10	U20	U10	U20	U10	U20
CTRL	11	201	0.0	8.0	0.0	0.0	0.0	0.0	18	26
SEED_GL	26	206	70	12	15	5.4	136	2.7	41	26
SEED_GH	47	206	90	12	36	5.3	327	2.6	41	27
SEED_AL	58	356	96	74	48	155	429	77	8.2	21
SEED_AH	16	303	38	45	5.2	102	47	51	32	51

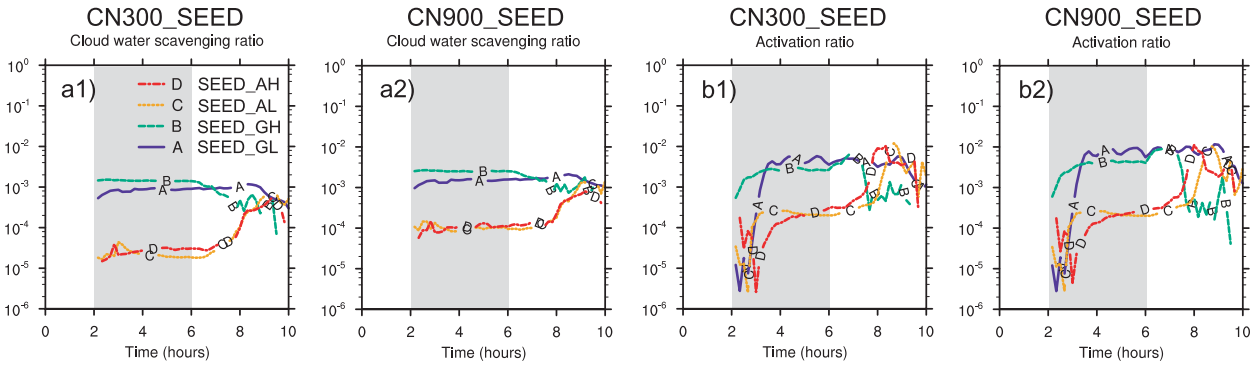

FIG. 11. Time series of AgI scavenging ratio by cloud water for (a1) CN300_SEED and (a2) CN900_SEED and AgI activation ratio for (b1) CN300_SEED and (b2) CN900_SEED. Curves A–D indicate SEED_GL, SEED_GH, SEED_AL, and SEED_AH, respectively. The seeding period is indicated by the gray area in each plot.

mode in airborne seeding cases was deposition, which is not significantly affected by cloud droplet concentration. Thus, the local AgI activation ratios of airborne seeding cases did not change much between CN300 and CN900.

The reduced precipitation and increased SPR of orographic precipitating clouds associated with increasing pollution level in the atmosphere was simulated by the model (Table 8), which is in agreement with many recent numerical studies (Muhlbauer et al. 2010; Xue et al. 2010, 2012; Saleeby et al. 2011). When the air was very polluted (CN900), the C–C process was almost shut down (99% snow ratio in the CN900_CTRL case as listed in Table 8). It is shown in Table 8 that precipitation enhancements by AgI seeding were greater under polluted conditions than in the clean (BASE) case (Table 2). Reisin et al. (1996) and Givati and Rosenfeld (2005) also showed that the seeding effect is positively related to the pollution level. Patterns of SPR changes induced by seeding that are similar to those of the BASE experiments were observed as well.

When the background IN concentration was very low (IN001), natural precipitation processes became weaker and resulted in less precipitation than in the BASE control case (cf. Table 2 with Table 9). The reverse was true when conditions representing dust storms were simulated (IN100). The fact that seeding effects became stronger in the IN001 cases (weaker in the IN100 cases) relative to the BASE seeding cases is expected given the lack of (abundance of) natural ice nuclei in the air and thus weaker (stronger) ice-related microphysical processes. The impacts on the SPR by seeding were also similar to those of the BASE simulations.

f. *Seeding rate effects*

As seen in the analyses of the experiments described in previous sections, seeding consistently increased accumulated precipitation on the ground under a variety of conditions. Given this result, it is useful to study the relationship between seeding rate and precipitation enhancement. A set of experiments with multiple seeding rates for both ground-based and airborne seeding addresses this question. Nucleation rates, scavenging rates, and activation ratios for the GH cases using different seeding rates are shown in Fig. 12, similar to Fig. 5. It is found that nucleation rates of all four modes were positively related to seeding rates. The maximum increase of immersion freezing (SR1K) was not as prominent as in the other modes, however. This result was partly caused by the reduced scavenging ratio of the AgI particles (Fig. 12b1) and was partly caused by the reduced CCN activation ratio, which was limited by the available water vapor close to the ground (not shown). Figures 12b1 and 12b3 show that when the seeding rate was very large (SR1K) the cloud water scavenging and AgI activation

TABLE 8. As in Table 2, but for CN300 and CN900.

Case	P (mm)		R_{snow} (%)		$P - P_{ctrl}$ (mm)		$(P - P_{ctrl})/P_{ctrl}$ (%)		SPR (%)	
	CN300	CN900	CN300	CN900	CN300	CN900	CN300	CN900	CN300	CN900
CTRL	66	35	64	99	0.0	0.0	0.0	0.0	25	35
SEED_GL	82	57	73	100	16	22	24	63	35	52
SEED_GH	83	55	73	100	17	20	26	58	36	51
SEED_AL	179	166	96	100	113	131	172	377	11	12
SEED_AH	146	124	91	100	80	89	122	256	22	26

TABLE 9. As in Table 2, but for IN001 and IN100.

Case	P (mm)		R_{snow} (%)		$P - P_{ctrl}$ (mm)		$(P - P_{ctrl})/P_{ctrl}$ (%)		SPR (%)	
	IN001	IN100	IN001	IN100	IN001	IN100	IN001	IN100	IN001	IN100
CTRL	83	133	2.4	71	0.0	0.0	0.0	0.0	15	13
SEED_GL	97	139	20	73	13	5.4	16	4.1	23	15
SEED_GH	97	141	20	73	14	7.7	17	5.8	23	17
SEED_AL	188	205	86	93	105	72	126	54	10	10
SEED_AH	159	182	66	82	75	48	91	36	18	16

ratios decreased relative to other seeding rates, which indicates that a maximum AgI activation number was reached, limited by the available vapor and cloud water.

For the AH cases (Fig. 13), deposition was still the dominant mode of ice nucleation and only the deposition rate increased with increasing seeding rate. As mentioned in section 4a, the AgI particles from airborne seeding entered an ice-supersaturated region before reaching the supercooled liquid water. These AgI acted as deposition ice nuclei first, which made the deposition rate scale with the seeding rate. The fast-growing ice crystals that were nucleated through deposition of AgI particles depleted vapor and water quickly. The available vapor and water could only sustain a fixed amount of AgI acting as ice nuclei through other modes, which resulted in the activation rates of other modes remaining almost constant regardless of the seeding rates (Figs. 13a1–4). Similar to what was seen for ground-based seeding, the AgI activation number was also limited by available vapor and cloud water (Figs. 13b1 and 13b3).

As a consequence of the increasing nucleation rates of AgI particles, precipitation enhancements increased with increasing seeding rates for all seeding cases (Table 10). The relationships between relative precipitation enhancements (%) and seeding rate ratios (relative to the default rate) for all of the seeding rate cases and the BASE_SEED cases are demonstrated in Fig. 14. A power-law function fits very well to the data from both ground-based seeding cases and airborne seeding cases. To examine the robustness of the power-law relationship, additional SR experiments under various conditions were performed using the soundings of T273, RH90, Z1KM, N008, and U20. These tests showed that the power law indeed describes the relationship between seeding rate and seeding effect very well; the correlation coefficient was always greater than 0.9 for

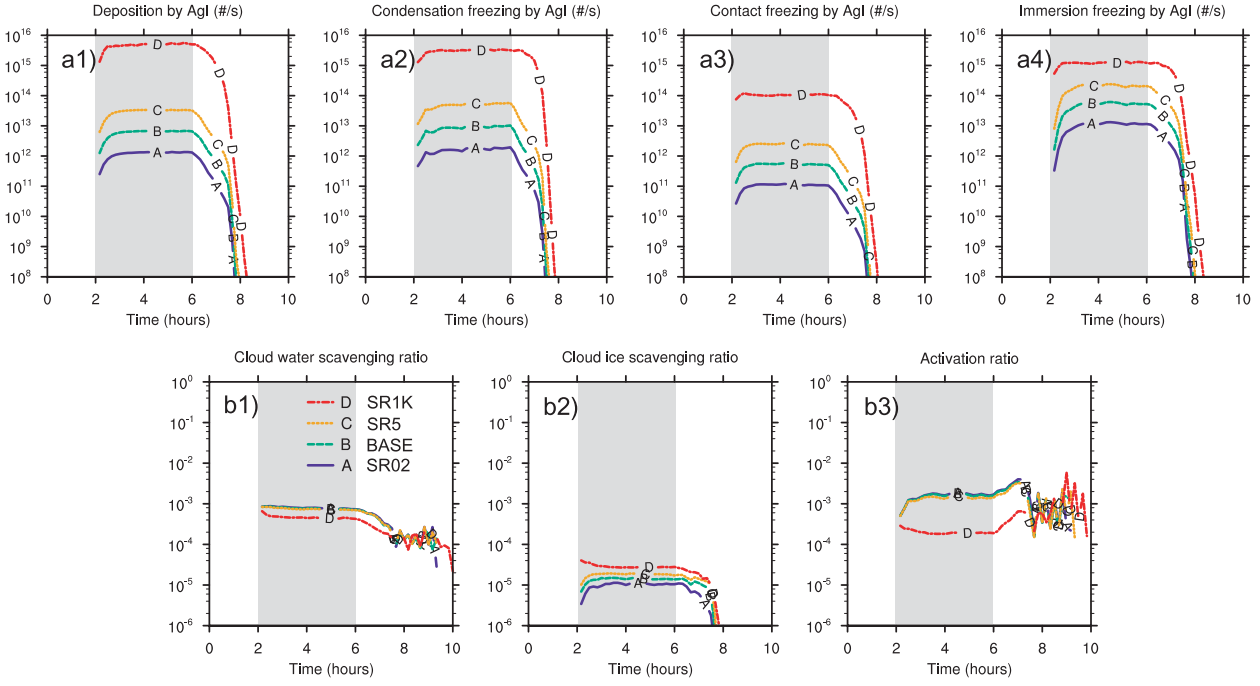

FIG. 12. As in Fig. 5, but for different GH seeding rate cases. Curves A–D indicate SR02_SEED_GH, BASE_SEED_GH, SR5_SEED_GH, and SR1K_SEED_GH, respectively.

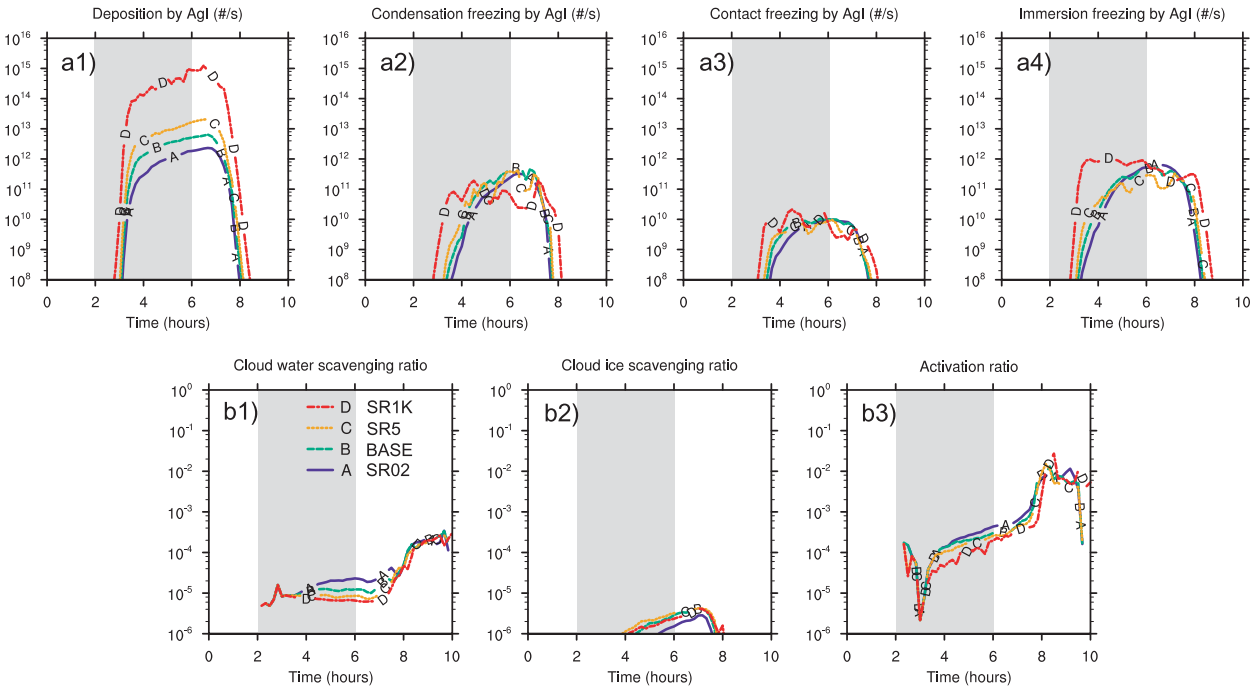

FIG. 13. As in Fig. 12, but for different AH seeding rate cases.

ground-based seeding cases and was almost always greater than 0.8 for airborne seeding cases.

If we assume that 1000 times the default seeding rate is the upper limit of AgI that can be released into the air, the seeding effect of a particular seeding rate can be calculated by these regressions. The plots clearly show that airborne seeding in these experiments was much more efficient than ground-based seeding. Even at 1/5 of the default seeding rate, airborne seeding enhanced precipitation more than did ground-based seeding with 100 times the default seeding rate. Consequently, the apparent seeding effect of airborne seeding rendered it less sensitive to varying seeding rates than that of ground-based seeding (i.e., the slopes of the data for the ground-based seeding cases are steeper than those for the airborne seeding cases). These relations are based on 2D simulations in which the airborne (ground) seeding effects can be overestimated (underestimated), however, and the continuous increase of seeding effect with increasing seeding rate may be a result of model artifacts (see discussions in next section). Nonetheless, such information of seeding effect versus seeding rate can be used in cost–benefit analyses to support decision making in seeding operations.

5. Discussion

The traditional picture of how glaciogenic seeding works is based on laboratory studies by Schaefer (1946) and Vonnegut (1947) such that seeding materials nucleate ice crystals and subsequently deplete the liquid water through the Bergeron–Findeisen process. These newly formed ice particles are believed to grow faster to precipitation size than without the seeding agent. From then on, the existence of supercooled liquid water became a necessary condition for glaciogenic seeding practices.

TABLE 10. As in Table 2, but for SR02, SR5, and SR1K.

Case	P (mm)			R_{snow} (%)			$P - P_{ctrl}$ (mm)			$(P - P_{ctrl})/P_{ctrl}$ (%)			SPR (%)		
	SR02	SR5	SR1K	SR02	SR5	SR1K	SR02	SR5	SR1K	SR02	SR5	SR1K	SR02	SR5	SR1K
CTRL	101	101	101	34	34	34	0.0	0.0	0.0	0.0	0.0	0.0	17	17	17
SEED_GL	107	117	167	38	46	75	5.7	16	66	5.6	16	65	20	23	26
SEED_GH	109	120	163	39	48	72	7.8	19	62	7.7	19	61	21	25	24
SEED_AL	189	198	208	88	89	90	88	97	108	87	96	107	11	10	9.5
SEED_AH	153	176	188	67	77	84	52	75	87	51	75	86	20	16	13

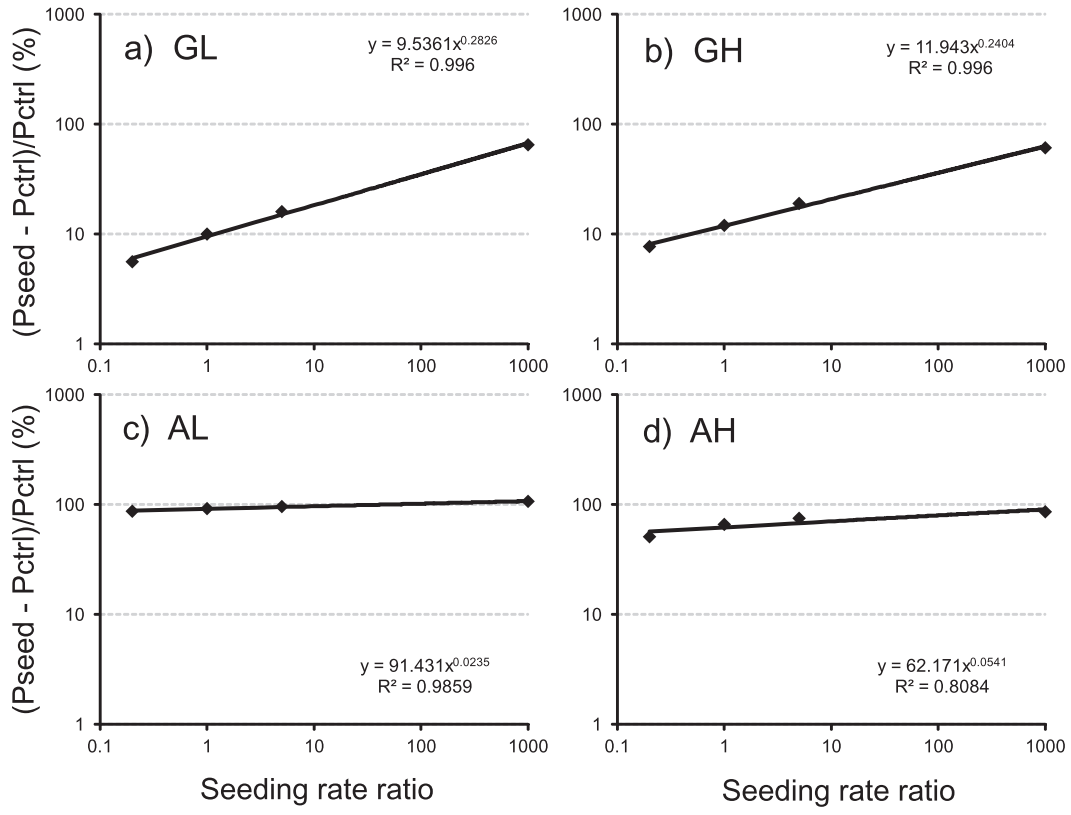

FIG. 14. Scatterplots of the relative precipitation enhancement by seeding (%) as a function of seeding rate ratio (relative to the default seeding rate: ratios of 0.2, 1, 5, and 1000 are shown in the plot) for (a) GL, (b) GH, (c) AL, and (d) AH. The axis scales of these plots are log–log. Power-law regression lines are fit to each plot.

The analyses presented here, however, showed that most of the precipitation enhancement by seeding is from the depletion of vapor (deposition growth of ice particles) in the air (see Fig. 4). Under the same conditions, the ice saturation ratio is always greater than the water saturation ratio. Therefore, the ice-supersaturated region is always greater than liquid water volume as seen from Figs. 3, 6, 7, 8, and so on. Once the AgI particles enter the high ice-supersaturated region ($S_i > 1.04$), ice crystals will be nucleated through deposition mode and will grow by deposition as simulated by all AL cases. Hence, we suggest use of a necessary condition of $S_i > 1.04$ to replace the original necessary condition of presence of supercooled liquid water in cloud-seeding operations. A forthcoming paper will address this issue.

The activation rates of deposition, condensation freezing, and immersion freezing of AgI particles are direct functions of ambient temperature [see Eqs. (1), (2), and (4)]. It has been shown that when the surface temperature was 278 K the maximum local AgI activation ratio was above 1% in ground-based seeding cases (CN900 in Fig. 11) and was about 2% in airborne seeding cases. To find out how this ratio changes with temperature, we performed extra experiments with surface temperature of 268 (T268) and 263 K (T263). The local AgI activation ratios of T273, T268, and T263 are illustrated in Figs. 15a–c. It is shown that the local AgI activation ratio did not increase with decreasing surface temperature all of the time. The maximum value was around 60% in the T268_AH case. This value was found after hour 7, however, when the AgI–cloud interactions were not steady. When the temperature was very cold (T263), the natural clouds depleted most of the vapor and resulted in a steady local AgI activation ratio of 0.1%. Some high activation ratios around 2% were observed in the early stage of seeding, which is more representative than the values after hour 7. Further tests in which we directly injected AgI particles into the supercooled liquid cloud region at hour 3 under different surface temperatures (i.e., the SLW_SEED cases in Fig. 15d) showed results that are similar to those in Figs. 15a–c. The local AgI activation ratio reached a maximum value of 40% in the T268 case and remained balanced at 0.1% in T263. The seeding effects were negligible in these high activation ratio cases (relative precipitation enhancements were less than 1%), however, because of

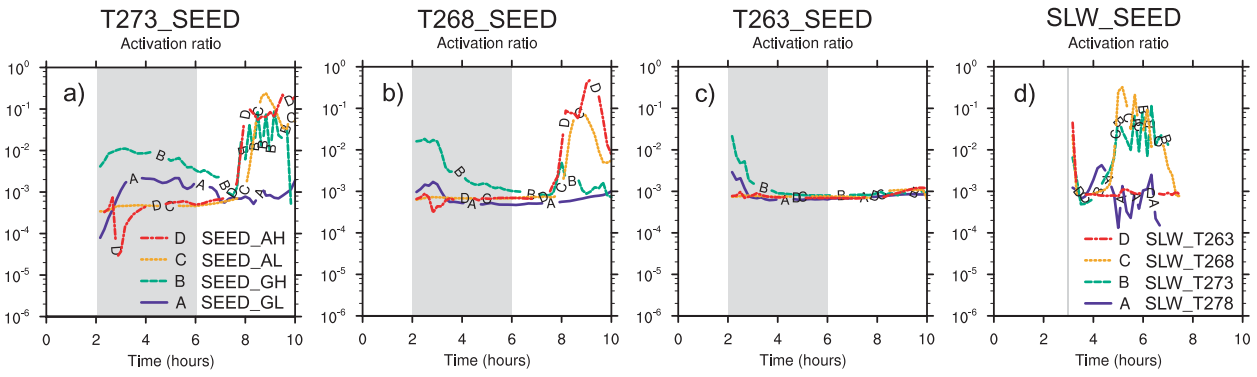

FIG. 15. Time series of AgI activation ratio for (a) T273, (b) T268, (c) T263, and (d) SLW seeding experiments. Curves A–D in (a)–(c) represent GL, GH, AL, and AH. Curves A–D in (d) indicate surface temperatures of 278, 273, 268, and 263 K. A pulse of AgI with the same amount as in other seeding cases was released into the entire liquid cloud region at hour 3 in SLW cases. The seeding period is indicated by the gray area in each plot.

efficient ice-phase microphysical processes in the very cold clouds. The analyses indicate that the local AgI activation ratio is between 0.02% and 2% in orographic clouds under most seeding conditions.

It has been demonstrated in section 4f that the relative precipitation enhancement increased with increasing seeding rates. It will be helpful to seeding operations if a relationship between seeding effect and meteorological conditions or cloud macro-/microphysical properties can be found. After exploring the relationships between seeding effect and many different parameters (total precipitation, snow ratio, moist Brunt–Väisälä frequency, and spillover ratio), we found that the seeding effect was highly anticorrelated with total precipitation of the CTRL case (natural precipitation). Figure 16 shows that the power law again accurately describes the relationship between seeding effects and natural precipitation amounts. The size of the symbol represents the average LWC of the cloud.[6] CN300 and CN900 are in yellow and red, respectively, while IN001 and IN100 are in light blue and dark blue, respectively. The experiments of T283 and N005 were excluded when calculating the regressions because T283 is a warm-rain case for which glaciogenic seeding is not appropriate and N005 is a convective case, which is in a regime other than the stable stratified orographic cloud investigated in this study. For AH, RH70, Z1KM, and U10 were also excluded because of their very low cloud top, which made AH seeding not comparable to other seeding scenarios. These excluded cases are indicated by open circles in Fig. 16. It is shown that the natural precipitation was not strongly dependent on the average LWC. The effect of changing IN was not as prominent as the change of CN on the natural precipitation. The physical interpretation of this relationship is that the more efficient the natural precipitation processes are, the less seeding effect is obtained. Precipitation is the process of turning water vapor in the air into water or ice on the ground. If the natural cloud is very good at this process, it will leave less vapor with which cloud seeding can work, which translates into less of a seeding effect. A similar argument has been raised by many previous studies (Young 1996; Reisin et al. 1996; Li and Pitter 1997; List 2004; Givati and Rosenfeld 2005). Therefore, identifying clouds with low precipitation efficiency is important in seeding operations.

All of the experiments performed in this study showed that simulated cloud seeding enhanced the precipitation amount on the ground, but at certain locations the precipitation was reduced (see curve C at 420 km in Fig. 4c1). The location of precipitation enhancement is very important in reality. If the extra precipitation falls on different sides of the mountain, the water will flow into different watersheds and will have an impact on the local water resource usage. Figure 17 illustrates the differences of spillover ratio in percentage between the seeding and the control cases for all cases except for T283, N005 (for the same reasons as mentioned in the previous paragraph), SR02, SR5, and SR1K. Note that the ground-based seeding technique increased the SPR for all experiments, which means that the majority of precipitation enhancement was located on the lee side of the mountain.[7] The lower-flight-track airborne seeding

[6] The average LWC was calculated for cloudy volume with LWC $> 0.01\ g\ kg^{-1}$ over the entire simulation period, and it ranged from $0.25\ g\ kg^{-1}$ for N005 to $0.44\ g\ kg^{-1}$ for U20.

[7] Upwind precipitation was also enhanced but not as prominently as downwind enhancements (see Fig. 4c1).

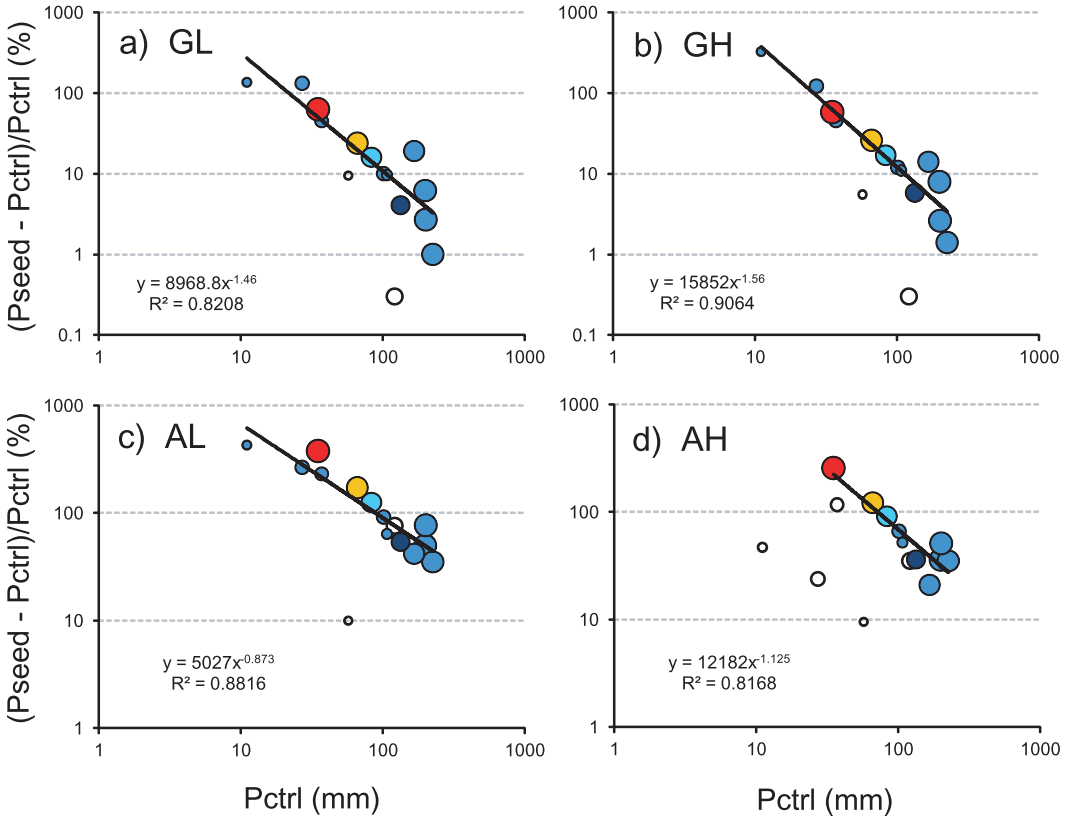

FIG. 16. Scatterplots of the relative precipitation enhancement by seeding (%) as a function of CTRL total precipitation (mm). The relative size of the symbol indicates the average LWC ($g\,kg^{-1}$) of the case. CN300 and CN900 are filled with yellow and red, respectively. IN001 and IN100 are in light blue and dark blue, respectively. For GL, GH, and AL, open circles indicate data from the T283 and N005 cases. For AH, open circles indicate data from the T283, RH70, Z1KM, N005, and U10 cases. The regressions are based on the color-filled data points.

reduced the SPR for all experiments, indicating a windward-side precipitation enhancement. There is no consistent trend of the SPR change in the higher-flight-track airborne seeding cases. It is apparent from this plot that the type of seeding method should be chosen according to the requirements of the precipitation-enhancement location in seeding operations.

Because of the limitations of the microphysics scheme and two-dimensionality used in this study, some results were only valid to a certain degree and need to be interpreted carefully. Aerosol activation as a function of local vertical velocity, temperature, pressure, aerosol size, and chemistry yields a greatly variable droplet concentration even when aerosol concentrations are horizontally and vertically uniform. As discussed in section 4a, the constant concentration of cloud droplets arbitrarily reduced the scavenging process and suppressed the contact-freezing mode. This assumption also impacts riming and diffusion processes. Riming is more efficient when cloud droplets are large (Saleeby et al. 2011; Xue et al. 2012a). The constant droplet concentration increases the droplet size when cloud water increases and hence arbitrarily enhances the riming efficiency. In a similar way, the fixed concentration and increased droplet size reduce the total water surface area, thus weakening the Bergeron–Findeisen process in the cloudy area. With these limitations in mind, the continuous increase of the seeding effect with an increase of seeding materials as shown in the seeding rate tests should be limited at a lower seeding rate. In reality, overseeding might occur when extreme amounts of IN are injected into a cloud (Durant et al. 2008). Therefore, we do not recommend using as much seeding materials as possible in cloud-seeding operations. Nonetheless, increasing the number of ground generators and their coverage area is suggested. To tackle the problems affected by model artifacts, a more sophisticated microphysics scheme simulating detailed aerosol activation and aerosol–cloud interactions should be used. A new version of this AgI cloud-seeding parameterization that is based on a detailed bin microphysics scheme is under development (Xue et al. 2012). The new scheme will be used to

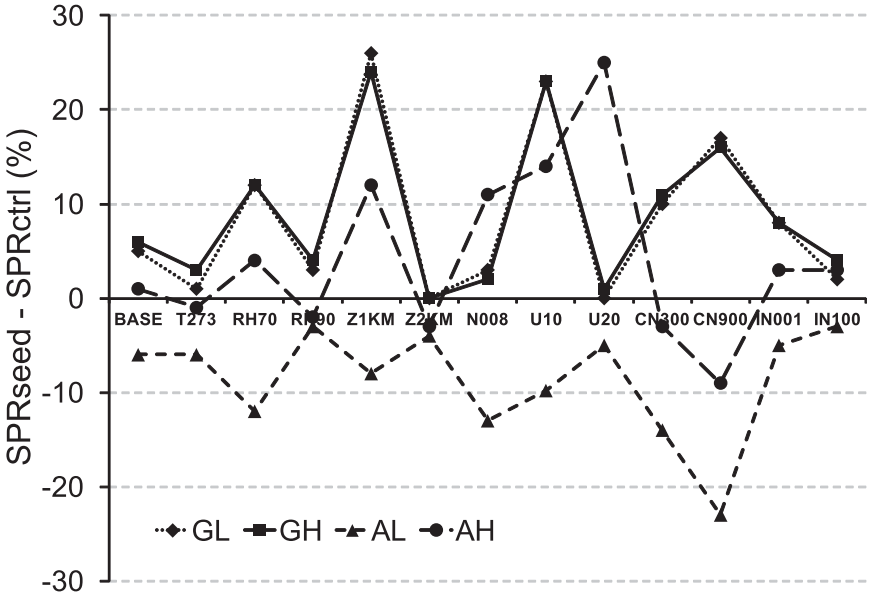

FIG. 17. The differences of the spillover ratio (%) between the seeding cases and the CTRL cases for BASE, T273, RH70, RH90, Z1KM, Z2KM, N008, U10, U20, CN300, CN900, IN001, and IN100 experiments. Each line connects each experiment for one of GL, GH, AL, or AH.

investigate seeding events in more detail and to validate and improve the current bulk version. The lack of the third dimension and smooth topography strongly suppressed the AgI dispersion, resulting in high immersion-freezing nucleation rates (see section 4a) and weak vertical dispersion of AgI particles in ground-based seeding cases. The limited cloud region being affected by ground-based seeding led to underestimations of the seeding effect. As detailed in Part II, such limitations are relieved when a 3D model setup and real topography were used.

6. Conclusions

The wintertime orographic seeding effects have been investigated by simulating 2D idealized mixed-phase cloud formation over a bell-shaped mountain using an AgI cloud-seeding parameterization embedded in the Thompson microphysics scheme of the WRF model. By varying the meteorological conditions, cloud microphysical properties, and seeding rates, the sensitivity of seeding effects of four seeding scenarios, including lower/higher groups of ground generators and lower/higher flight tracks, have been explored. The analyses of the cloud macro- and microphysical properties and precipitation features showed that this AgI cloud-seeding parameterization was able to reasonably simulate the physical chain of events that results from cloud seeding. Caution should be used when interpreting the results, however, given the limitations of the constant cloud droplet concentration assumed in the scheme and the two-dimensional model setup. The seeding effects of all seeding scenarios for all cases are summarized in Table 11. It is clearly shown that glaciogenic seeding does not work well in convective orographic clouds. Ground-based seeding should be avoided when surface temperatures are high, clouds are very deep, winds are strong, background IN is high, and/or the seeding rate is low. Whenever it is possible, a lower-altitude flight track rather than a higher track is suggested for airborne seeding. The five main conclusions of this study are as follows:

1) Deposition was the dominant nucleation mode of AgI particles from aircraft seeding, and immersion freezing was the most active mode from ground-based seeding. Deposition and condensation freezing were also important for ground-based seeding. Contact freezing was the weakest nucleation mode for both ground-based and airborne seeding.
2) Through diffusion and riming processes, ice crystals nucleated by AgI particles depleted vapor and liquid water, resulting in more ice-phase precipitation on the ground for all seeding cases relative to natural precipitation. Most of the precipitation enhancement came from vapor depletion rather than liquid water consumption. The relative precipitation enhancement by seeding ranged from 0.3% to 429% under various conditions.

TABLE 11. Summary of the seeding effects of all seeding scenarios. The plus and minus symbols indicate that the absolute precipitation enhancement by the seeding location is greater than or no greater than 10 mm, respectively (first four columns), the relative precipitation enhancement by the seeding location is greater than or no greater than 10%, respectively (the four center columns), or that there is upwind or downwind precipitation enhancement, respectively, relative to the mountain peak (the last four columns).

	$\Delta P > 10$ mm				$\Delta P/P > 10\%$				Upwind			
Case	GL	GH	AL	AH	GL	GH	AL	AH	GL	GH	AL	AH
BASE	+	+	+	+	+	+	+	+	−	−	+	−
T273	+	+	+	+	+	+	+	+	−	−	+	+
T283	−	−	+	+	−	−	+	+	−	−	+	−
RH70	+	+	+	+	+	+	+	+	−	−	+	−
RH90	+	+	+	+	−	−	+	+	−	−	+	+
Z1KM	+	+	+	−	+	+	+	−	−	−	+	−
Z2KM	−	−	+	+	−	−	+	+	−	−	+	+
N008	+	+	+	+	+	+	+	+	−	−	+	−
N005	−	−	−	−	−	−	−	−	+	+	+	+
U10	+	+	+	−	+	+	+	−	−	−	+	−
U20	−	−	+	+	−	−	+	+	−	−	+	−
CN300	+	+	+	+	+	+	+	+	−	−	+	+
CN900	+	+	+	+	+	+	+	+	−	−	+	+
IN001	+	+	+	+	+	+	+	+	−	−	+	−
IN100	−	−	+	+	−	−	+	+	−	−	+	−
SR02	−	−	+	+	−	−	+	+	−	−	+	−
SR5	+	+	+	+	+	+	+	+	−	−	+	+
SR1K	+	+	+	+	+	+	+	+	−	−	+	+

3) The maximum local AgI activation ratio was about 60% under optimum conditions. Under most seeding conditions, however, this ratio was between 0.02% and 2% in orographic clouds.
4) The seeding effect was inversely related to the natural precipitation efficiency but was positively related to seeding rates.
5) Ground-based seeding was shown to enhance precipitation on the lee side of the mountain, whereas airborne seeding from the lower-altitude flight track enhanced precipitation on the windward side of the mountain.

The 2D idealized simulations performed in this study can reasonably simulate the physical processes associated with orographic glaciogenic seeding events, although some limitations exist. To better examine the seeding processes, a more sophisticated microphysics scheme should be used. The 3D simulations of real cloud-seeding events with sensitivity tests using the same AgI cloud-seeding parameterization will be presented in Part II.

Acknowledgments. This study was partly supported by the NCAR Advanced Study Program, the Wyoming Water Development Commission as part of the Wyoming Weather Modification Pilot Program, and the Idaho Power Company. The development of the AgI cloud-seeding point-source module was supported by the Japanese Cloud Seeding Experiments for Precipitation Augmentation (JCSEPA) project of the Japanese Meteorological Research Institute. The authors greatly appreciate the comments and suggestions of the anonymous reviewers, which significantly improved the quality of the manuscript. All rights to the underlying data collected and/or generated with funding from the Wyoming Water Development Office (WWDO) from which this paper was created remain with the WWDO. This paper does not constitute the opinions of the State of Wyoming, the Wyoming Water Development Commission, or the Wyoming Water Development Office.

REFERENCES

Baines, P. G., 1995: *Topographic Effects in Stratified Flows*. Cambridge University Press, 500 pp.

Breed, D., M. Pocernich, R. Rasmussen, B. Boe, and B. Lawrence, 2011: Evaluation of the Wyoming winter orographic cloud seeding program: Design of the randomized seeding experiment. Preprints, *18th Conf. on Planned and Inadvertent Weather Modification,* Seattle, WA, Amer. Meteor. Soc., 2.1. [Available online at https://ams.confex.com/ams/91Annual/webprogram/Paper180664.html.]

Bruintjes, R. T., 1999: A review of cloud seeding experiments to enhance precipitation and some new prospects. *Bull. Amer. Meteor. Soc.,* **80,** 805–820.

Caro, D., W. Wobrock, A. I. Flossmann, and N. Chaumerliac, 2004: A two-moment parameterization of aerosol nucleation and impaction scavenging for a warm cloud microphysics: Description and results from a two-dimensional simulation. *Atmos. Res.,* **70,** 171–208.

Chai, S. K., W. G. Finnegan, and R. L. Pitter, 1993: An interpretation of the mechanisms of ice-crystal formation operative in the Lake Almanor cloud-seeding program. *J. Appl. Meteor.,* **32,** 1726–1732.

Chen, B., and H. Xiao, 2010: Silver iodide seeding impact on the microphysics and dynamics of convective clouds in the high plains. *Atmos. Res.,* **96,** 186–207.

Cooper, W. A., 1986: Ice initiation in natural clouds. *Precipitation Enhancement: A Scientific Challenge, Meteor. Monogr.,* No. 43, Amer. Meteor. Soc., 29–32.

Curic, M., D. Janc, and V. Vuckovic, 2007: Cloud seeding impact on precipitation as revealed by cloud-resolving mesoscale model. *Meteor. Atmos. Phys.,* **95,** 179–193.

DeMott, P. J., 1995: Quantitative descriptions of ice formation mechanisms of silver iodide-type aerosols. *Atmos. Res.,* **38,** 63–99.

Dennis, A. S., 1980: *Weather Modification by Cloud Seeding.* Academic Press, 275 pp.

Deshler, T., and D. W. Reynolds, 1990: The persistence of seeding effects in a winter orographic cloud seeded with silver iodide burned in acetone. *J. Appl. Meteor.,* **29,** 477–488.

——, ——, and A. W. Huggins, 1990: Physical response of winter orographic clouds over the Sierra Nevada to airborne seeding using dry ice or silver iodide. *J. Appl. Meteor.,* **29,** 288–330.

Durant, A. J., R. A. Shaw, W. I. Rose, Y. Mi, and G. G. Ernst, 2008: Ice nucleation and overseeding of ice in volcanic clouds. *J. Geophys. Res.,* **113,** D09206, doi:10.1029/2007JD009064.

Gabriel, K. R., 1999: Ratio statistics for randomized experiments in precipitation stimulation. *J. Appl. Meteor.,* **38,** 290–301.

Geerts, B., Q. Miao, Y. Yang, R. Rasmussen, and D. Breed, 2010: An airborne profiling radar study of the impact of glaciogenic cloud seeding on snowfall from winter orographic clouds. *J. Atmos. Sci.,* **67,** 3286–3302.

——, ——, and ——, 2011: Boundary layer turbulence and orographic precipitation growth in cold clouds: Evidence from profiling airborne radar data. *J. Atmos. Sci.,* **68,** 2344–2365.

Givati, A., and D. Rosenfeld, 2005: Separation between cloud-seeding and air-pollution effects. *J. Appl. Meteor.,* **44,** 1298–1314.

Guo, X., G. Zheng, and D. Jin, 2006: A numerical comparison study of cloud seeding by silver iodide and liquid carbon dioxide. *Atmos. Res.,* **79,** 183–226.

Hashimoto, A., S. Satake, T. Kato, and M. Murakami, 2008: Numerical simulation of the ground-based AgI seeding (in Japanese). *Proc. 2008 Autumn Meeting of the MSJ,* Sendai, Japan, Meteorological Society of Japan, B359.

Holroyd, E. W., J. A. Heimbach, and A. B. Super, 1995: Observations and model simulation of AgI seeding within a winter storm over Utah's Wasatch Plateau. *J. Wea. Modif.,* **27,** 35–56.

Huggins, A. W., 2007: Another wintertime cloud seeding case study with strong evidence of seeding effects. *J. Wea. Modif.,* **39,** 9–36.

Langer, G., 1986: Feasibility study of silver iodide smoke as an atmospheric dispersion tracer for Rocky Flats plant site. U.S. Department of Energy Tech. Rep. DOE/TIC-4500, 14 pp.

Li, Z., and R. L. Pitter, 1997: Numerical comparison of two ice crystal formation mechanisms on snowfall enhancement from ground-based aerosol generators. *J. Appl. Meteor.,* **36,** 70–85.

List, R., 2004: Weather modification—A scenario for the future. *Bull. Amer. Meteor. Soc.,* **85,** 51–63.

Liu, C., K. Ikeda, G. Thompson, R. Rasmussen, and J. Dudhia, 2011: High-resolution simulations of wintertime precipitation in the Colorado Headwaters region: Sensitivity to physics parameterizations. *Mon. Wea. Rev.,* **139,** 3533–3553.

Liu, Y.-B., and Coauthors, 2008: The operational mesogamma-scale analysis and forecast system of the U.S. Army Test and Evaluation Command. Part I: Overview of the modeling system, the forecast products, and how the products are used. *J. Appl. Meteor. Climatol.,* **47,** 1077–1092.

Manton, M. J., and L. Warren, 2011: A confirmatory snowfall enhancement project in the Snowy Mountains of Australia. Part II: Primary and associated analyses. *J. Appl. Meteor. Climatol.,* **50,** 1448–1458.

——, ——, S. L. Kenyon, A. D. Peace, S. P. Bilish, and K. Kemsley, 2011: A confirmatory snowfall enhancement project in the Snowy Mountains of Australia. Part I: Project design and response variables. *J. Appl. Meteor. Climatol.,* **50,** 1432–1447.

Meyers, M. P., P. J. DeMott, and W. R. Cotton, 1995: A comparison of seeded and nonseeded orographic cloud simulations with an explicit cloud model. *J. Appl. Meteor.,* **34,** 834–846.

Muhlbauer, A., T. Hashino, L. Xue, A. Teller, U. Lohmann, R. M. Rasmussen, I. Geresdi, and Z. Pan, 2010: Intercomparison of aerosol-cloud-precipitation interactions in stratiform orographic mixed-phase clouds. *Atmos. Chem. Phys.,* **10,** 8173–8196.

National Research Council, 2003: *Critical Issues in Weather Modification Research.* National Academy Press, 131 pp.

Pitter, R. L., and H. R. Pruppacher, 1973: A wind tunnel investigation of the evolution of the freezing of small water drops falling at terminal velocity in air. *Quart. J. Roy. Meteor. Soc.,* **99,** 540–551.

Qiu, J., and D. Cressey, 2008: Taming the sky. *Science,* **453,** 970–974.

Rasmussen, R. M., and Coauthors, 2011: High-resolution coupled climate runoff simulations of seasonal snowfall over Colorado: A process study of current and warmer climate. *J. Climate,* **24,** 3015–3048.

Rauber, R. M., R. D. Elliott, J. O. Rhea, A. W. Huggins, and D. W. Reynolds, 1988: A diagnostic technique for targeting during airborne seeding experiments in wintertime storms over the Sierra Nevada. *J. Appl. Meteor.,* **27,** 811–828.

Reisin, T., Z. Levin, and S. Tzivion, 1996: Rain production in convective clouds as simulated in an axisymmetric model with detailed microphysics. Part I: Description of the model. *J. Atmos. Sci.,* **53,** 497–519.

Reynolds, D. W., and A. S. Dennis, 1986: A review of the Sierra Cooperative Pilot Project. *Bull. Amer. Meteor. Soc.,* **67,** 513–523.

Saleeby, S. M., W. R. Cotton, and J. D. Fuller, 2011: The cumulative impact of cloud droplet nucleating aerosols on orographic snowfall in Colorado. *J. Appl. Meteor. Climatol.,* **50,** 604–625.

Schaefer, V. J., 1946: The production of ice crystals in a cloud of supercooled water droplets. *Science,* **104,** 457–459.

Super, A. B., 1999: Summary of the NOAA/Utah Atmospheric Modification Program: 1990–1998. *J. Wea. Modif.,* **31,** 51–75.

——, and B. A. Boe, 1988: Microphysical effects of wintertime cloud seeding with silver iodide over the Rocky Mountains. Part III: Observations over the Grand Mesa, Colorado. *J. Appl. Meteor.,* **27,** 1166–1182.

——, and J. A. Heimbach, 1988: Microphysical effects of wintertime cloud seeding with silver iodide over the Rocky Mountains. Part II: Observations over the Bridger Range, Montana. *J. Appl. Meteor.,* **27,** 1153–1165.

Thompson, G., R. Rasmussen, and K. Manning, 2004: Explicit forecasts of winter precipitation using an improved bulk microphysics scheme. Part I: Description and sensitivity analysis. *Mon. Wea. Rev.,* **132,** 519–542.

——, P. R. Field, W. R. Hall, and R. Rasmussen, 2008: Explicit forecasts of winter precipitation using an improved bulk microphysics scheme. Part II: Implementation of a new snow parameterization. *Mon. Wea. Rev.,* **136,** 5095–5115.

Vonnegut, B., 1947: The nucleation of ice formation by silver iodide. *J. Appl. Phys.,* **18,** 593–595.

Warburton, J. A., R. H. Stone, and B. L. Marler, 1995a: How the transport and dispersion of AgI aerosols may affect detectability of seeding effects by statistical methods. *J. Appl. Meteor.,* **34,** 1929–1941.

——, L. G. Young, and R. H. Stone, 1995b: Assessment of seeding effects in snowpack augmentation programs: Ice nucleation and scavenging of seeding aerosols. *J. Appl. Meteor.,* **34,** 121–130.

Xue, L., A. Teller, R. M. Rasmussen, I. Geresdi, and Z. Pan, 2010: Effects of aerosol solubility and regeneration on warm-phase orographic clouds and precipitation simulated by a detailed bin microphysical scheme. *J. Atmos. Sci.,* **67,** 3336–3354.

——, ——, ——, ——, ——, and X. Liu, 2012: Effects of aerosol solubility and regeneration on mixed-phase orographic clouds and precipitation. *J. Atmos. Sci.,* **69,** 1994–2010.

——, S. Tessendorf, E. Nelson, R. Rasmussen, D. Breed, S. Parkinson, P. Holbrook, and D. Blestrud, 2013: Implementation of a silver iodide cloud-seeding parameterization in WRF. Part II: 3D simulations of actual seeding events and sensitivity tests. *J. Appl. Meteor. Climatol.,* **52,** 1458–1476.

Yin, Y., Z. Levin, T. G. Reisin, and S. Tzivion, 2000: Seeding convective clouds with hygroscopic flares: Numerical simulations using a cloud model with detailed microphysics. *J. Appl. Meteor.,* **39,** 1460–1472.

Young, K. C., 1996: Weather modification—A theoretician's viewpoint. *Bull. Amer. Meteor. Soc.,* **77,** 2701–2710.